The isotopic composition of atmospheric nitrous oxide observed at the high-altitude research station Jungfraujoch, Switzerland

Longfei Yu[1*], Eliza Harris[1†], Stephan Henne[1], Sarah Eggleston[1], Martin Steinbacher[1], Lukas Emmenegger[1], Christoph Zellweger[1] and Joachim Mohn[1]

[1]Laboratory for Air Pollution & Environmental Technology, Empa, Swiss Federal Laboratories for Materials Science and Technology, Ueberlandstr. 129, CH-8600 Duebendorf, Switzerland.

[†]Current address: Institute of Ecology, University of Innsbruck, Sternwartestrasse 15, A-6020 Innsbruck, Austria

[*] Correspondence: L. Yu (longfei.yu@empa.ch)

Abstract

Atmospheric nitrous oxide (N_2O) levels have been continuously growing since preindustrial times. Mitigation requires information about sources and sinks on the regional and global scales. Isotopic composition of N_2O in the atmosphere could contribute valuable constraints. However, isotopic records of N_2O in the unpolluted atmosphere remain too scarce for large-scale N_2O models. Here, we report the results of discrete air samples collected weekly to bi-weekly over a five-year period at the high-altitude research station Jungfraujoch, located in central Switzerland. High-precision N_2O isotopic measurements were made using a recently developed preconcentration-laser spectroscopy technique. The measurements of discrete samples were accompanied by *in situ* continuous measurements of N_2O mixing ratios. Our results indicate a pronounced seasonal pattern with minimum N_2O mixing ratios in late summer, associated with a maximum in $\delta^{15}N^{bulk}$ and a minimum in intramolecular ^{15}N site preference ($\delta^{15}N^{SP}$). This pattern is most likely due to stratosphere-troposphere exchange (STE), which delivers N_2O-depleted but ^{15}N-enriched air from the stratosphere into the troposphere. Variability in $\delta^{15}N^{SP}$ induced by changes in STE may be masked by biogeochemical N_2O production processes in late summer, which are possibly dominated by a low-$\delta^{15}N^{SP}$ pathway of N_2O production (denitrification), providing an explanation for the observed seasonality of $\delta^{15}N^{SP}$. Footprint analyses and atmospheric transport simulations of N_2O for Jungfraujoch suggest that regional emissions from the planetary boundary layer contribute to seasonal variations of atmospheric N_2O isotopic composition at Jungfraujoch, albeit more clearly for $\delta^{15}N^{SP}$ and $\delta^{18}O$ than for $\delta^{15}N^{bulk}$. With the time-series of five years, we obtained a significant interannual trend for $\delta^{15}N^{bulk}$ after deseasonalization (-0.052±0.012‰ a^{-1}), indicating that the atmospheric N_2O increase is due to isotopically depleted N_2O sources. We estimated the average isotopic signature of anthropogenic N_2O sources with a two-box model to be -8.6±0.6‰

for $\delta^{15}N^{bulk}$, 34.8±3‰ for $\delta^{18}O$ and 10.7±4‰ for $\delta^{15}N^{SP}$. Our study demonstrates that seasonal variation of N_2O isotopic composition in the background atmosphere is important when determining interannual trends. More frequent, high-precision and inter-laboratory compatible measurements of atmospheric N_2O isotopocules, especially for $\delta^{15}N^{SP}$, are needed to better constrain anthropogenic N_2O sources, and thus the contribution of biogeochemical processes to N_2O growth on the global scale.

1 Introduction

Nitrous oxide (N_2O) is a potent greenhouse gas (Fowler et al., 2015) and a strong stratospheric ozone-depleting substance (Ravishankara et al., 2009). For several decades, near-surface atmospheric N_2O mixing ratios have been continuously measured at a series of remote sites, within the networks of the Global Atmosphere Watch Programme (JMA and WMO, 2018), the Advanced Global Atmospheric Gases Experiment (AGAGE) (Prinn et al., 2018), and the National Oceanic and Atmospheric Administration (NOAA) Earth System Research Laboratory (ESRL) Global Monitoring Division (GMD) (Nevison et al., 2011). These measurements have shown a significant increase in atmospheric N_2O mixing ratio, at a current growth rate of about 0.93 nmol mol^{-1} a^{-1} (WMO, 2018). On the global scale, given excessive nitrogen (N) fertilizer application, agriculture is known to be the largest and most important anthropogenic source of N_2O (Reay et al., 2012; Tian et al., 2019). However, long-term observations of N_2O in the unpolluted atmosphere have shown seasonal and interannual variabilities as well as interhemispheric differences in N_2O mixing ratios (Nevison et al., 2011; Thompson et al., 2014a, 2014b), which cannot yet be resolved by atmospheric transport models and existing emission inventories. Moreover, regional contributions of N_2O emissions and the strengths of individual N_2O production pathways remain difficult to quantify.

Isotopic signatures of atmospheric N_2O can provide important constraints on N_2O sources (Denk et al., 2017) and trends (Kim and Craig, 1993). The ratios of $^{15}N/^{14}N$ and $^{18}O/^{16}O$ in N_2O are often reported in δ notation as $\delta(^{15}N/^{14}N)$ and $\delta(^{18}O/^{16}O)$, abbreviated as $\delta^{15}N^{bulk}$ (average for $^{14}N^{15}N^{16}O$ and $^{15}N^{14}N^{16}O$) and $\delta^{18}O$, respectively. A large fraction of N_2O emitted to the atmosphere originates from soil bacterial processes, which usually emit N_2O that is more enriched in light (^{14}N, ^{16}O) isotopes than the tropospheric background (Pérez et al., 2001; Snider et al., 2015a; Toyoda et

al., 2017). By contrast, N_2O produced in the oceans (Bourbonnais et al., 2017; Fujii et al., 2013) and emitted from fossil fuel combustion (Ogawa and Yoshida, 2005; Toyoda et al., 2008) has higher $\delta^{15}N^{bulk}$ and $\delta^{18}O$ values which are comparable to the tropospheric background. A recent study has summarized isotopic signatures of anthropogenic N_2O sources divided into the EDGAR (Emissions Database for Global Atmospheric Research) emission categories (Janssens-Maenhout et al., 2019), showing differences in isotopic signatures between agricultural ($\delta^{15}N^{bulk}$ = -17.8 to -1.0‰ and $\delta^{18}O$ = 23.9 to 29‰) and industrial sources ($\delta^{15}N^{bulk}$ = -28.7 to 5.5‰ and $\delta^{18}O$ = 28.6 to 40.3‰) (Harris et al., 2017). These empirical ranges, together with isotopic mixing models, provide a valuable approach to interpret variability in atmospheric N_2O mixing ratios.

A number of studies have analyzed temporal trends in N_2O isotopic composition in the modern atmosphere (Kaiser et al., 2003; Park et al., 2012; Röckmann and Levin, 2005; Toyoda et al., 2013) and in the past from firn and ice cores (Bernard et al., 2006; Ishijima et al., 2007; Prokopiou et al., 2018; Röckmann et al., 2003; Sowers et al., 2002). These isotopic measurements have shown a decrease in both $\delta^{15}N^{bulk}$- and $\delta^{18}O$-N_2O associated with an increasing trend in atmospheric N_2O mixing ratios since preindustrial times, indicating that the recent increase of atmospheric N_2O may be due to agricultural emissions (^{15}N and ^{18}O depleted). The reported trend since the 1960s seems rather steady (-0.034±0.005 ‰ a^{-1} for $\delta^{15}N^{bulk}$ and -0.016 ‰±0.006 a^{-1} for $\delta^{18}O$) (Bernard et al., 2006; Ishijima et al., 2007; Park et al., 2012; Prokopiou et al., 2017; Röckmann et al., 2003; Röckmann and Levin, 2005). However, a more recent (1999-2010) study reported a smaller decreasing trend in $\delta^{15}N^{bulk}$ and only an insignificant trend in $\delta^{18}O$ for the Northern Hemisphere (Toyoda et al., 2013). Several hypotheses were proposed to explain the differences in the observed trends: 1) the interhemispheric difference in N_2O emission sources results in inconsistent isotopic signatures among different studies (Thompson et al., 2014b); 2) uncertainties in isotopic

86 measurements and variable sampling schemes (air type, sampling frequency and time) mask the
87 small secular trend of N_2O isotopic composition in the background atmosphere (Toyoda et al.,
88 2013); and/or 3) N_2O source isotopic signatures have changed in recent years, possibly due to
89 shifts in N fertilizer type and climatic forcing (Tian et al., 2019). Hence, further investigation into
90 the global N_2O source inventory and its evolution over time requires more frequent, precise
91 measurements of N_2O isotopocules in the unpolluted atmosphere, particularly in the Northern
92 Hemisphere.

93 Recently, site-specific composition of N_2O isotopomers (site preference: $\delta^{15}N^{SP}$), which denotes
94 the difference of ^{15}N between the central ($^{14}N^{15}N^{16}O$, α position) and terminal ($^{15}N^{14}N^{16}O$, β
95 position) N atoms, has been applied to constrain sources contributing to atmospheric N_2O (Toyoda
96 et al., 2013; Yoshida and Toyoda, 2000). $\delta^{15}N^{SP}$ of N_2O is particularly effective for distinguishing
97 between the major N_2O production processes, i.e. nitrification and denitrification, generally
98 referred to as aerobic and anaerobic N_2O production, with high and low $\delta^{15}N^{SP}$, respectively (Sutka
99 et al., 2006). However, despite the advantages of $\delta^{15}N^{SP}$ measurements, existing long-term studies
100 have not yet been able to reach a definitive understanding of the $\delta^{15}N^{SP}$-N_2O trend, showing both
101 positive (Bernard et al., 2006; Park et al., 2012; Röckmann and Levin, 2005) and negative
102 tendencies (Röckmann et al., 2003) over the last four decades. This is probably due to an
103 insufficient analytical precision and poor inter-laboratory agreement, in particular as the
104 aforementioned studies are all based on isotope ratio mass spectrometry (IRMS). To retrieve site-
105 specific isotopic information by IRMS, the N_2O^+ molecular ions and the NO^+ fragment ions are
106 analyzed and raw data have to be corrected for rearrangements of central and terminal N and ^{17}O
107 content (Toyoda et al., 2001). Inappropriate correction algorithms and the limited availability of

reference materials (Ostrom et al., 2018) further enlarge the analytical uncertainty (Mohn et al., 2014).

Seasonal variability in atmospheric N_2O isotopic composition, which could affect the longer-term trends, is still rarely reported in the literature (Park et al., 2012; Toyoda et al., 2013). Moreover, studies of seasonality of N_2O isotopic composition are limited to the recent past since the air samples derived from firn and ice cores suffer from coarse temporal resolution (< 2 samples per year). Park et al. (2012) studied seasonality of atmospheric N_2O isotopic composition by analyzing a set of archived air samples collected from Cape Grim (Australia) using a sophisticated mathematical modeling approach. They found consistent seasonal patterns in $\delta^{15}N^{bulk}$, $\delta^{18}O$ and $\delta^{15}N^{SP}$ of atmospheric N_2O, showing highest $^{15}N/^{18}O$ enrichment in June and lowest in December. This pattern was negatively correlated with the seasonality of the N_2O mixing ratios (lowest in April-May and highest in December), which is in agreement with a previous study by Nevison et al. (2011). The negative correlation between isotopic composition and mixing ratios has been explained by stratosphere-troposphere exchange (STE), which transports N_2O-depleted but isotopically enriched stratospheric air (prevailing reduction process) into the lower atmosphere (Yung and Miller, 1997). However, in a more recent study from Hateruma Island (Japan), Toyoda et al. (2013) reported insignificant seasonal patterns in atmospheric N_2O isotopocules (smaller variability than measurement precision), despite their finding of a somewhat similar seasonal pattern in N_2O mixing ratio (minimum in July). Although there are interhemispheric differences in N_2O sources and distinct sampling frequencies in the two studies discussed above (2-3 times per year versus monthly), it is noteworthy that both studies observed significantly larger variability in $\delta^{15}N^{SP}$ than in $\delta^{15}N^{bulk}$ and $\delta^{18}O$. Whether the fluctuations in $\delta^{15}N^{SP}$ are mainly caused by the

limited repeatability of the chosen analytical techniques or interplay of processes or mechanisms regulating atmospheric N_2O remains to be tested (Park et al., 2012).

With inherent selectiveness, in particular for site-specific isotopic composition, laser spectroscopy provides a new analytical approach for direct, precise measurements of all four N_2O isotopocules (Harris et al., 2014; Mohn et al., 2012). The recent development of quantum cascade laser absorption spectroscopy (QCLAS) coupled with an automated preconcentration unit has been applied to measure N_2O isotopocules in ambient air, with comparable precision for $\delta^{15}N^{bulk}$ and $\delta^{18}O$ and superior precision for $\delta^{15}N^{SP}$ relative to IRMS systems (Harris et al., 2017; Mohn et al., 2014). Here, we present results from the application of a preconcentration unit coupled to QCLAS to measure atmospheric N_2O isotopocules in background air collected at the high altitude research station Jungfraujoch, Switzerland. Between April 2014 and December 2018, we collected weekly to bi-weekly air samples for N_2O isotopic analyses, in parallel with online measurement of N_2O mixing ratios. To our knowledge, this work reports the first time-series of background atmospheric N_2O isotopic composition using laser spectroscopy. With this unique dataset, we aim to 1) constrain seasonal patterns of three N_2O isotopic signatures at the Jungfraujoch observatory; 2) determine interannual trends in N_2O isotopocules, especially $\delta^{15}N^{SP}$; and 3) interpret the observed patterns in N_2O mixing ratios using temporal trends in N_2O isotopic composition and reported isotopic signatures of anthropogenic sources.

2 Materials and Method

2.1 Site description

The high altitude research station Jungfraujoch (3580 m above sea level), located on the northern ridge of the Swiss Alps, is a well-established site for studying unpolluted atmosphere over Central Europe (e.g. Buchmann et al., 2016). Although the station is located in the free troposphere most of the time, it is occasionally affected by air recently lifted from the planetary boundary layer (Herrmann et al., 2015; Zellweger et al., 2003). Henne et al. (2010) investigated the representativeness of 35 European monitoring stations and categorized Jungfraujoch as "mostly remote". The Jungfraujoch station is part of several national and international networks, like the meteorological SwissMetNet network operated by MeteoSwiss, the Swiss National Air Pollution Monitoring Network (NABEL), the Global Atmospheric Watch Programme (GAW) of the World Meteorological Organization (WMO) and the Integrated Carbon Observation Systems (ICOS) Research Infrastructure. This results in an extended set of long-term and continuously available parameters such as meteorological variables (Appenzeller et al., 2008), greenhouse gases (Schibig et al., 2015; Sepúlveda et al., 2014; Yuan et al., 2018), CO_2 isotopic composition (Sturm et al., 2013; Tuzson et al., 2011), ozone-depleting substances and their replacement products (Reimann et al., 2008), atmospheric pollutants (Logan et al., 2012; Pandey Deolal et al., 2012; Zellweger et al., 2009) and aerosol parameters (Bukowiecki et al., 2016).

2.2 *In situ* measurements and discrete air sampling (flasks)

In situ observations of N_2O mixing ratios commenced at Jungfraujoch in December 2004. Initially, measurements were made with gas chromatograph (GC) (Agilent 6890N, USA) followed by electron capture detection (ECD). The time resolution of these measurements was 24 to 30 minutes.

In late 2014, we implemented a cavity-enhanced off-axis integrated cavity out-put spectroscopy analyzer (OA-ICOS, Los Gatos Research Inc., Mountain View, CA, USA), which measures the atmospheric N_2O mixing ratio continuously. Measurements of N_2O mixing ratios at Jungfraujoch were calibrated with three standard gases (319, 327 and 342 nmol mol^{-1}) and accompanied with measurement of a working standard (331 nmol mol^{-1}) every 160 minutes to account for instrumental drift. In addition, short- (two times every 40 hours) and long-term (every 40 hours) target measurements were included to monitor the data quality. Due to the superior measurement precision compared to the GC-ECD method (Lebegue et al., 2016), the OA-ICOS record has become the primary time-series since January 2015. The GC-ECD observations continued until summer 2016 for comparison and quality control.

Additional parameters, recorded within the NABEL network and the ICOS infrastructure, were included in the analysis below. These data were carbon monoxide (CO) (measured by cavity ring-down spectroscopy; Model G2401, Picarro Inc., USA), the sum of oxidized nitrogen species (NO_y) (measured by chemiluminescence detection after conversion of NO_y to NO on a heated gold catalyst; CLD 89p, Eco Physics, Switzerland) and O_3 (measured by UV absorption; TEI 49i, Thermo Scientific, USA). Details on measurement methods and calibration strategies can be found in Zellweger et al. (2009) for CO, Pandey Deolal et al. (2012) for NO_y and Logan et al. (2012) for O_3.

In conjunction with the online measurements, we deployed an automated sampling system (Fig. S1) to collect pressurized air samples in aluminum cylinders from the same air inlet at the Sphinx observatory of the Jungfraujoch station, for subsequent N_2O mixing ratio and isotopic analyses. The sample collection was conducted weekly from April 2014 to February 2016. After a sampling gap of five months due to a technical failure, we reinitiated a bi-weekly sampling, which continued

from August 2016 to December 2018. The sampling system, automated by a customized LabVIEW program (National Instruments Corp., USA), consisted of a Nafion drier (PD-100T-48MSS, Perma Pure LLC, USA), a membrane gas compressor (KNF Neuberger, USA; Type N286 series), a 16-port selector valve (EMT2CSD16MWEPH, VICI AG, Swtizerland), and a rack to accommodate nine 2-L aluminum flasks (Luxfer, Messer Schweiz AG, Switzerland). During sample filling, pre-evacuated flasks were first purged with ambient air five times (1 hour), and then filled to 12000 hPa within 40 min, resulting in approximately 24 L (298 K and 1000 hPa) of air per flask for isotopic analysis. Air sample filling generally took place between 2:00 and 3:00 pm local time at each sampling day. Sample flasks were sent back to the laboratory at Empa for analyses every few months. For this study, 142 air samples were collected in flasks and analyzed for N_2O isotopocules.

2.3 Analyses of discrete air samples

Discrete air samples were regularly analyzed in batches but note in chronological order to prevent the imprint of analytical drifts on temporal trends of the samples. N_2O mole fractions were analyzed by QCLAS (CW-QC-TILDAS-76-CS, Aerodyne Research Inc., USA) against NOAA standards on the WMO-X2006A calibration scale (Hall et al., 2007), at a precision around 0.1 nmol mol^{-1} (determined with the average of 1-min data).

The four most abundant N_2O isotopocules ($^{14}N^{14}N^{16}O$, 99.03%; $^{14}N^{15}N^{16}O$, 0.36%; $^{15}N^{14}N^{16}O$, 0.36%; $^{14}N^{14}N^{18}O$, 0.20%) were analyzed using a customized QCLAS system (Aerodyne Research, Inc., USA) (Heil et al., 2014) coupled with an automated preconcentration device (Mohn et al., 2010). Before entering the pre-concentration unit, sample air is passed through a Sofnocat 423 trap (Molecular Products Limited, GB) to remove CO, and subsequently through an Ascarite trap (Ascarite: 6 g, 10–35 mesh, Sigma Aldrich, Switzerland, bracketed by $Mg(ClO_4)_2$, 2 × 1.5 g, Alfa Aesar, Germany) to remove CO_2 and water. Approximately 5.5 L of air with a flow of 250 ml min^{-}

[1] (at 295 K and 3500 hPa) is then passed through a HayeSep D trap cooled to -145 °C to collect N_2O (Mohn et al., 2010). For N_2O release to the multipath cell of the QCLAS, the HayeSep D trap is quickly heated to 10 °C and flushed with high-purity synthetic air (20.5% of O_2 in N_2) carrier gas at a flow rate of 25 ml min^{-1} (at 295 K and 3500 hPa). A final cell pressure around 16 hPa is achieved, which results in an N_2O mixing ratio of about 45 μmol mol^{-1}. More instrumental details can be found in previous studies (Harris et al., 2017; Mohn et al., 2010, 2012). Sample tanks were each analyzed twice to yield duplicates for N_2O isotopic results, which left sufficient air for amount fraction analysis as described in the previous paragraph.

2.4 Data analyses

We used 10-minute averages of the continuous *in situ* measurements from the Jungfraujoch station across this study. For a point-to-point comparison of continuous and discrete measurements of N_2O mixing ratio, we aggregated 10-minute averages of *in situ* data for the same period when the discrete sample was filled into the cylinder (40 min).

In this study, we report abundances of N_2O isotopocules using δ notation (‰) as below:

$$\delta X = \frac{(R_{sample} - R_{standard})}{R_{standard}} \quad (1)$$

where X refers to $^{15}N^{\alpha}$ ($^{14}N^{15}N^{16}O$), $^{15}N^{\beta}$ ($^{15}N^{14}N^{16}O$) and ^{18}O ($^{14}N^{14}N^{18}O$); R refers to the ratio between the amount fractions of the rare isotopocules as mentioned above and the amount fraction of $^{14}N^{14}N^{16}O$; isotope standards refer to atmospheric N_2 for ^{15}N and Vienna Standard Mean Ocean Water (VSMOW) for ^{18}O.

Hence, the total ^{15}N content of N_2O and site-specific composition of N_2O isotopomers could be further illustrated as $\delta^{15}N^{bulk}$ and $\delta^{15}N^{SP}$, respectively, according to the equations below:

$$\delta^{15}N^{bulk} = (\delta^{15}N^{\alpha} + \delta^{15}N^{\beta})/2 \quad (2)$$

$$\delta^{15}N^{SP} = \delta^{15}N^{\alpha} - \delta^{15}N^{\beta} \quad (3)$$

Two standards (CG1 and CG2; in 79.5% N_2 and 20.5% O_2) with distinct isotopic signatures ($\delta^{15}N^{\alpha}$ = 16.29 ± 0.07‰ (CG1) and -51.09 ± 0.07‰ (CG2); $\delta^{15}N^{\beta}$ = -2.59 ± 0.06‰ and -48.12 ± 0.04‰; $\delta^{18}O$ = 39.37 ± 0.04‰ and 30.81 ± 0.03‰) were used for calibrating isotopic composition. The calibration gases CG1 and CG2 were calibrated on the Tokyo Institute of Technology (TIT) scale, based on cross-calibration with primary standards assigned by TIT (Mohn et al., 2012, 2014). In addition, CG1 was measured repeatedly between samples and target gases to account for instrumental drift. Both CG1 and CG2 have N_2O mixing ratios of 45 μmol mol^{-1}, similar to the N_2O amount fraction of the samples after preconcentration. However, to correct for possible instrumental dependence on N_2O mixing ratio, CG1 was diluted to N_2O mole fractions of 35-40 μmol mol^{-1} within each measurement batch. In general, duplicated isotopic measurements of flask samples yielded values of repeatability of 0.10-0.20‰ for $\delta^{15}N^{bulk}$ and $\delta^{18}O$, and 0.15-0.25‰ for $\delta^{15}N^{SP}$.

At the beginning of the project, a batch of three cylinders (50 L water volume, Luxfer, Italy) were filled with pressurized ambient air in Dübendorf with an oil-free, three stage compressor (SA-3, Rix Industries, USA) and used as long-term target gases. The pressurized ambient air target gas was analyzed with identical treatment as Jungfraujoch air samples during every analysis batch, to monitor long-term analytical drift. Standard deviations for repeated target gas measurements throughout the period of Jungfraujoch sample measurements, were 0.13‰ for $\delta^{15}N^{bulk}$, 0.21‰ for $\delta^{15}N^{SP}$, and 0.11‰ for $\delta^{18}O$ (Fig. S2).

2.5 Surface air footprint analysis and simulated regional N_2O enhancement

We analyzed the air mass origin at Jungfraujoch by applying the Lagrangian particle dispersion model (LPDM) FLEX-PART in the backward mode (Stohl et al., 2005). The model was driven by meteorological fields taken from the ECMWF-IFS operational analysis cycle, extracted at a resolution of 1°×1°, 90/137 levels globally, and at higher horizontal resolution of 0.2°×0.2° for central Europe. We released 50000 virtual air parcels every 3 hours at 3000 m a.s.l. from Jungfraujoch to perform backward dispersion simulations over 10 days, which allowed us to calculate surface source sensitivities (concentration footprints). A release height of 3000 m a.s.l. was previously determined to be an optimum for simulating concentration footprints at Jungfraujoch, given the stated horizontal resolution which results in a considerable smoothing of the complex, alpine orography (Keller et al., 2012). The 3-hourly surface footprints for the whole observation period were used to categorize different transport regimes using the clustering approach outlined in Sturm et al. (2013). This allowed us to distinguish among six different source regions: Free Troposphere (FT), Southwest (SW), East (E), Local (L), West (W) and Northwest (NW).

Similar to Henne et al. (2016) for CH_4 and based on spatially resolved N_2O emission inventories (Meteotest for Switzerland; EDGAR for Europe), we used the FLEXPART concentration footprints to calculate time-series of atmospheric mole fraction increases at Jungfraujoch resolved by emission sectors (Henne et al., 2016). The emission inventory by Meteotest consists of 12 emission sectors, among which all sectors except “organic soils” are comparable to sectors in the EDGAR inventory (See Table 1) (Janssens-Maenhout et al., 2019). To improve seasonal representation of the emissions in our model, we used a monthly resolved, optimized version of the emission inventory, which was obtained through inverse modeling using the N_2O atmospheric mole fractions observed between March 2017 and September 2018 at the tall tower site

Beromuenster on the Swiss plateau (Henne et al., 2019). Therefore, in this study, source contributions to Jungfraujoch were estimated specifically for the period mentioned above.

2.6 Evaluation of seasonal pattern and interannual trend for time-series

To explore seasonality and interannual trends, we fit the time-series of *in situ* measurements of N_2O and O_3 mixing ratios, NO_y-to-CO ratios and isotopic measurements of N_2O with polynomial functions and Fourier series (four harmonics for *in situ* measurements and two harmonics for discrete measurements) (Thoning et al., 1989). Time-series were then decomposed into a linear trend, seasonal variability (per 12 months) and residuals. This fit was conducted with a nonlinear least-squares (NLS) model with R-3.5.3 (R Core Team, 2016). The detrended seasonality was examined by comparing peak-to-peak amplitudes with our analytical precisions and the uncertainty given by the one standard deviation of monthly residuals. To determine interannual trends, a linear regression was applied to both the raw and the deseasonalized datasets. The significance level is set to $p < 0.01$. The interannual trends for N_2O mixing ratios were found to be little affected by seasonality, so growth rates were determined only based on the raw datasets.

Although Jungfraujoch is a remote site, episodic influence from the planetary boundary layer can be observed at the station (Pandey Deolal et al., 2012; Zellweger et al., 2003). For evaluating trends of N_2O mixing ratio measurements, we filtered out *in situ* data with significant influence of plenary boundary layer, in order to represent a major air mass footprint from the free troposphere (FT). In addition to the air transport regimes, an alternative filtering criterion for the free troposphere was based on the published mean ranges of NO_y mixing ratios (501-748 pmol mol^{-1} depending on the season) and NO_y to CO ratios (0.003-0.005 depending on the season) at Jungfraujoch (Zellweger et al., 2003). This criterion is less strict than that given by footprint analyses (Herrmann et al.,

2015). After applying this criterion to the isotopic time-series (which led to the exclusion of 32 measurement points), we re-evaluated the seasonal and interannual trends in the N_2O isotopic composition. In addition, because of the strong variability observed for isotopic data during the first 1.5 years (until February 2016), we performed an independent evaluation for the time-series starting from August 2016.

2.7 Two-box model simulation

A two-box model representing a well-mixed troposphere and stratosphere was used to estimate the anthropogenic N_2O source strength and isotopic composition from the trends measured at Jungfraujoch, similar to the approaches used by several previous studies (Ishijima et al., 2007; Röckmann et al., 2003; Schilt et al., 2014; Sowers et al., 2002). The input variables used to run the model are given in Table 2. 200 iterations of the model were run using a Monte Carlo-style approach to approximate the uncertainty considering the uncertainty distribution for each input variable as given in Table 2. All variables were set independently within the Monte Carlo approximation except for preindustrial N_2O life time (τ_{PI}), which was fixed to 106% of the present-day N_2O life time τ_{PD} (Prather et al., 2015).

Within each iteration of the model, the preindustrial N_2O burden was first described, assuming steady state in the preindustrial era. The preindustrial stratospheric N_2O mixing ratio ($c_{S,PI}$) (270±7.5 nmol mol^{-1}) was taken from Sowers et al. (2002):

$$0 = F_{ex}\left(c_{PI} - c_{S,PI}\right) - (M_{PI} + M_{S,PI})/\tau_{PI} \quad (4)$$

where F_{ex} refers to the troposphere-stratosphere exchange rate; c_{PI} refers to the preindustrial tropospheric N_2O mixing ratio; and M_{PI} and $M_{S,PI}$ are the masses of N_2O in the troposphere and stratosphere respectively. The preindustrial terrestrial flux in Sowers et al. (2002) (equation 2) was

used here assuming no anthropogenic emissions. The delta values for the preindustrial stratosphere and the fractionation factor for the stratospheric sink were taken from equations 6 and 7 from Sowers et al. (2002) assuming steady state and no anthropogenic emissions. The model was run with a yearly time step starting from the preindustrial assuming that anthropogenic emissions began in 1845 (Sowers et al., 2002). For each year of the model run, the anthropogenic flux was calculated according to the exponential increase described by Sowers et al. (2002):

$$F_{\text{anth},t} = e^{\alpha(t-t_0)} - 1 \quad (5)$$

where t is the current year, t_0 = 1845 and α is the growth rate (assumed to be constant). The rates of change for tropospheric and stratospheric N_2O mixing ratios were then retrieved from equations 2 and 3 in Sowers et al. (2002), and for the isotopic composition of stratospheric and tropospheric N_2O from equations 6 and 7 in Sowers et al. (2002).

The values of the parameters describing the anthropogenic flux were optimized to fit both the trend and the absolute values for the five years of Jungfraujoch isotope data, and the mixing ratio data from the Jungfraujoch flasks and *in situ* data since 2005 (GAW data source). The uncertainties in α and in the anthropogenic source isotopic signatures were approximated by one standard deviation of values derived from repeated model runs.

2.8 Evaluation of the combined effects from STE and soil emission on $\delta^{15}N^{SP}$

To evaluate the combined effects of STE and soil emission on the seasonal variability of $\delta^{15}N^{SP}$ (i.e. August minima), we made a mixing calculation as below:

Soil emission: Based on the determined seasonality of N_2O mole fraction at Jungfraujoch, the maximum N_2O mole fraction enhancement was approximately 0.2 nmol mol^{-1} above baseline (Fig.

1). Hence, we assumed N_2O enhancement from soil emission to be close to 0.15 to 0.20 nmol mol^{-1}, which is close to the maximum N_2O enhancement in our observation. The isotopic effect from soil emission can be derived from the difference between soil emission (7.2‰; Table 1) and tropospheric air (18‰, Fig. 2) in $\delta^{15}N^{SP}$, i.e. -10.8‰.

Mixing with stratospheric air: The minimum of N_2O mole fraction in August (-0.20 nmol mol^{-1}) is likely to be the result of both N_2O mole fraction enhancement from soil emission and N_2O mole fraction depletion due to STE. Given the assumed N_2O enhancement from soil emission, we estimated the N_2O depletion due to STE as -0.35 to -0.40 nmol mol^{-1}. The isotopic effect due to mixing with stratospheric air can be approximated using the apparent isotopic fractionation ε_{app} (Kaiser et al., 2006), which was derived from the slope of Rayleigh plot with normalized N_2O mole and isotope ratios. For $^{15}N^{SP}$, ε_{app} is calculated from the difference between $^{15}N/^{14}N$ isotope fractionations at the central and terminal N atoms, i.e. ${}^{\alpha}\varepsilon_{app}$ - ${}^{\beta}\varepsilon_{app}$. Therefore, for the lower stratosphere, ε_{app} ($^{15}N^{SP}$) was calculated to be about -15‰ (see more details in Kaiser et al., 2006).

Overall effect: Combing the isotope effects and contributions to the change of N_2O mole fraction by the two processes, the net effect is [(-0.35 to -0.40 nmol mol^{-1}) (-15‰) + (0.15 to 0.20 nmol mol^{-1}) (-10.8‰)] / (330 nmol mol^{-1}) $\approx$ 0.01‰. Such isotope effect is below our analytical precision and too small to be measured in the background atmosphere.

2.9 "Bottom-up" estimates of source isotopic signatures

To gauge the accuracy of the two-box model, we deployed a "bottom-up" approach as an alternative method of estimating the N_2O source signatures. The isotopic signatures of most N_2O source sectors given in the Meteotest/EDGAR emission inventory are available from the literature, except for the "Refinery" (Table 1). As "Refinery" generally contributes only about 0.02% of the

369 N_2O emission at Jungfraujoch, it was excluded for source isotopic signature estimation. The
370 simulated N_2O emissions by variable sources were categorized according to the EDGAR emission
371 types (Janssens-Maenhout et al., 2019). We then calculated isotopic signatures for the overall
372 source and the anthropogenic sources alone (excluding indirect natural emission) as weighted
373 averages.

3 Results

3.1 Atmospheric N_2O mixing ratios at Jungfraujoch

We observed a linear growth of atmospheric N_2O at Jungfraujoch during the period 2014-2018 (Fig. 1a). A point-to-point comparison of discrete and *in situ* measurements showed good agreement, in particular after the first year (2015-2018), where the data quality of *in situ* measurements was largely improved due to the implementation of the more precise laser spectroscopy method as compared to GC-ECD (Fig. 1b). The improvement in analytical precision for N_2O mixing ratio was due to better temporal coverage by the OA-ICOS instrument, in contrast with the GC analyses which conduct one measurement per 24-30 minutes. The annual growth rates from 2014 to 2018 determined with *in situ* measurements were 0.880 ± 0.001 and 0.993 ± 0.001 nmol mol^{-1} a^{-1} with and without GC-ECD measurements in 2014, respectively. This difference in N_2O growth rates is probably due to the limited data quality of GC-ECD, although a lower growth rate in 2014 compared to 2015-2018 cannot be excluded. It is noteworthy that the N_2O growth rate determined for 2015 to 2019 at Jungfraujoch is slightly above the global mean growth rate for the recent decade reported by NOAA (0.93 ± 0.03 nmol mol^{-1} a^{-1}) (WMO, 2018). If we filter the *in situ* dataset to examine only the "free troposphere" periods, we obtain a lower increase (0.858±0.002 nmol mol^{-1} a^{-1}). By comparison, the absolute growth rate determined from the discrete gas samples was even lower albeit larger uncertainty (0.813 ± 0.027 nmol mol^{-1} a^{-1}).

A significant seasonal pattern was observed for N_2O mixing ratios measured *in situ*, with a maximum in early summer and a minimum in late summer (Fig. 1c). For discrete N_2O measurements a similar trend was observed, but the detrended seasonality was not significant (Fig. S3), which might be due to the much lower number of samples.

3.2 Interannual trends of N_2O isotopic composition and anthropogenic source signatures

Time-series of $\delta^{15}N^{bulk}$, $\delta^{15}N^{SP}$ and $\delta^{18}O$ for atmospheric N_2O at Jungfraujoch are shown in Figure 2. The NLS model simulation accounts well for the variabilities of isotopic time-series. Interannual trends of three isotopic deltas were determined for both raw and deseasonalized datasets by linear regression (Table 3). The deseasonalized interannual trends were slightly smaller than the trends determined with the raw datasets. For the whole dataset, the deseasonalized trend indicates a significant decrease in $\delta^{15}N^{bulk}$, of -0.052±0.012‰ a^{-1}. In contrast, deseasonalized time-series of $\delta^{15}N^{SP}$ and $\delta^{18}O$ increased, albeit insignificantly, by 0.065±0.027‰ a^{-1} and 0.019±0.011‰ a^{-1}, respectively. The trends determined for periods with major air mass footprints from the free troposphere were close to those calculated for the whole dataset, except that $\delta^{15}N^{SP}$ trends decreased after filtering out the samples with significant impact from plenary boundary layer. This indicates that N_2O interannual trends observed at Jungfraujoch are of regional relevance, despite the fact that a small impact from local sources can be seen. Because of the observed irregular variability and the change in sampling frequency (though no change in daily sampling time) in our dataset, we separated the time-series into two phases: April 2014-February 2016 (first phase; weekly sampling) and August 2016-December 2018 (second phase; bi-weekly sampling). In the first phase, the rates of increase in $\delta^{15}N^{SP}$ and $\delta^{18}O$ were almost one order of magnitude larger than over the whole dataset. This is most likely due to the unexpectedly low $\delta^{15}N^{SP}$ and $\delta^{18}O$ in summer 2014 followed by a distinct increase in winter 2014-2015, which results in large rates of increase over short periods. Such growth rates were not seen in the second phase, when both $\delta^{15}N^{SP}$ and $\delta^{18}O$ showed small and insignificant variations. $\delta^{15}N^{bulk}$ displayed a decreasing interannual trend in both phases; however, the rate of decrease was larger in the second phase (-0.130±0.045‰ a^{-1}).

We tuned our two-box model to best match the observed N_2O mixing ratios and isotopic composition at Jungfraujoch. An estimate of anthropogenic emissions and source signatures is given in Table 4. For 2018, annual N_2O emissions were estimated to be 8.6±0.6 Tg N_2O-N a^{-1} equivalents. The average isotopic signatures for anthropogenic sources were -8.6±4‰, 34.8±3‰ and 10.7±4‰ for $\delta^{15}N^{bulk}$, $\delta^{15}N^{SP}$ and $\delta^{18}O$, respectively, which are clearly lower than those for preindustrial N_2O in the tropospheric background (Table 2; Toyoda et al., 2013).

3.3 Seasonal variation of N_2O isotopic composition

$\delta^{15}N^{SP}$ of N_2O showed the most pronounced variability among all isotopic time-series (Fig. 2), spanning 2.5‰ for individual flask sample measurements. Seasonal variability was estimated with the NLS model and presented as mean seasonal cycles (Fig. 3). For $\delta^{15}N^{SP}$ a "summer minimum" was found regardless of whether the entire dataset or only the second phase was considered (Fig. 3), although seasonal variability of the second time-series was smaller and showed the minimum occurring earlier. The seasonal pattern of $\delta^{15}N^{bulk}$ determined from the whole dataset indicates a significant summer maximum, but this was not seen when only the data from the second phase was taken, as there was no significant seasonal pattern over this period alone. For $\delta^{18}O$, we observed only small temporal variability and a lack of seasonal pattern. In addition, seasonal variations of time-series filtered for free troposphere were evaluated; these show temporal patterns similar to the whole dataset (Fig. 3).

3.4 Air mass origin and *in situ* measurements at Jungfraujoch

Back-trajectory simulations indicate six major transport clusters during 2014-2018, as shown in Figure 4a. Four of these transport regimes (SW, E, L and NW) dominate, accounting for about 60-90% coverage of the whole period. By contrast, the free troposphere cluster only represents 10-

20% of the data. Averaged monthly contributions of transport clusters are shown in Figure 4b, with more pronounced impact by the L, E and NW regions in summer and stronger contribution by FT and SW in winter. The source patterns of the air masses at Jungfraujoch were generally consistent across the years in the present study. However, an apparent discrepancy was found for discrete sampling times in the last two years (e.g. particularly low contribution from SW) which is most likely due to the low and variable sampling frequency of the discrete sample collection (Fig. 4b).

The detrended seasonal variability of *in situ* measurements indicates summer maxima for NO_y mixing ratios as well as NO_y-to-CO ratios at Jungfraujoch (Fig. 5). This likely indicates stronger exchange with the polluted planetary boundary layer in summer (Herrmann et al., 2015; Zellweger et al., 2003), which is consistent with the seasonal pattern of air mass footprint derived from back-trajectory simulations. The late spring-to-summer maxima for O_3 mixing ratios may be attributed to air mixing with stratosphere and/or planetary boundary layer, similar to the findings from a previous study at Jungfraujoch (Tarasova et al., 2009). On the other hand, CO shows a maximum in early spring and decreases in summer when its atmospheric lifetime is shortest. Atmospheric O_3, NO_y and CO measurements during our discrete sampling periods also well represented seasonal variability shown for *in situ* measurements, except for 2016-2017 where there was a five-month sampling gap (Fig. 5).

Comparisons of air mass footprints as well as O_3, NO_y and CO mixing ratios between *in situ* and discrete sampling indicate that the discrete sampling covers the main air source regions and variabilities in local pollution/free troposphere fairly well (Figs. 4 and 5). In the second phase (2016-2018), the less frequent sampling impedes evaluation of the seasonal and interannual variabilities.

3.5 Relationship between N_2O isotopic signatures and air mass footprints

We categorized N_2O mixing ratio and isotopic signature time-series into subsets based on the six air mass transport clusters. One-way ANOVA among clusters indicates that N_2O mixing ratios in air masses originating from cluster L were significantly higher and those from clusters FT and W were significantly lower than the others (Fig. 6). In accordance with the pattern found for mixing ratios, $\delta^{15}N^{SP}$ and $\delta^{18}O$ were high for cluster FT, and low for cluster L. For $\delta^{15}N^{bulk}$, little difference between transport clusters was detected.

4 Discussion

4.1 Quality assurance of isotopic measurements

This study reports the first results of background N_2O isotopic measurements based on a laser spectroscopic technique. Benefiting from the preconcentration process, we achieved measurement repeatability for a target gas of 0.10-0.20‰ for $\delta^{15}N^{bulk}$ and $\delta^{18}O$ (Fig. S2), which is comparable to that of IRMS measurements of ambient atmosphere (Park et al., 2012; Prokopiou et al., 2017; Röckmann et al., 2003; Toyoda et al., 2013). The long-term robustness of our technique is adequate for disentangling both seasonal and interannual temporal variability as shown in Figure 2. In particular, our repeatability of target measurements for $\delta^{15}N^{SP}$ (0.15-0.25‰) appears to be better than previous studies measuring background atmosphere or firn air (0.8‰, Park et al., 2012; 0.3‰, Prokopiou et al., 2017; 0.3‰, Toyoda et al., 2013).

4.2 Seasonal variabilities of atmospheric N_2O isotopic composition

In situ measurements of N_2O mixing ratios showed a clear early summer maximum and late summer minimum (Fig. 1). Such a seasonal pattern was previously found for a number of NOAA and AGAGE sites analyzing long-term N_2O records in the NH (Jiang et al., 2007; Nevison et al., 2011). One explanation of the late-summer minimum is a strong influence of the STE process in this period, which transports N_2O-depleted but isotopically enriched air downward from the stratosphere into the troposphere (Park et al., 2012; Snider et al., 2015b). During the late summer at Jungfraujoch, we find strong enrichment of ^{15}N in atmospheric N_2O according to the detrended seasonality for the whole dataset (Fig. 3). This is supported by a FLEXPART model simulation of the contribution of upper tropospheric air to Jungfraujoch station, showing highest contributions in August (Fig. S4; Henne et al., Personal Communication). At Hateruma Island, Japan, Toyoda

et al. (2013) observed a seasonal pattern of atmospheric N_2O mixing ratios which is comparable with our study, but found insignificant variations of isotopic composition. On the other hand, N_2O seasonal variability could be influenced by oceanic emission sources (Jiang et al., 2007; Nevison et al., 2005), complicating the explanations for the observed temporal patterns. For example, in another study looking at archived air from Cape Grim, Australia, Park et al. (2012) detected an April-May minimum and a November-December maximum for N_2O. This is expected for the SH, as STE is most prevalent in April (Nevison et al., 2011). They observed negative correlations of $\delta^{15}N^{bulk}$, $\delta^{15}N^{\alpha}$ and $\delta^{18}O$ with N_2O mixing ratios, appearing to support the idea that the STE process is responsible for seasonal variabilities in N_2O mixing ratios and isotopic composition at Cape Grim. However, the seasonal cycle for $\delta^{15}N^{\alpha}$ was much larger than $\delta^{15}N^{bulk}$ and $\delta^{18}O$, which could not be explained by STE alone. They suggested that the seasonal patterns of N_2O isotopes at Cape Grim may be due to mixing between oceanic sources (high N_2O with low ^{15}N and ^{18}O) and STE (low N_2O with high ^{15}N and ^{18}O) (Nevison et al., 2011; Park et al., 2012). However, because we observed a concurrent minimum of $\delta^{15}N^{SP}$ and maximum of $\delta^{15}N^{bulk}$ in July-August with low N_2O at Jungfraujoch (Fig. 3), additional mechanisms must be considered here.

Regional model simulations based on Swiss N_2O emissions derived from the inverse method were used to explore contributions from different sources to the variability in N_2O enhancements at Jungfraujoch. As shown in Figure 7a&7b, soil emissions, including direct and indirect emissions from agricultural lands and emissions from (semi-)natural areas, account for more than 70% of the total N_2O enhancements, while manure and waste management contribute another 20%. Total N_2O enhancements appeared to be highest in May to July (Fig. 7c), in accordance with the highest contribution by soil emissions. The early-to-middle summer maximum in the simulated N_2O enhancements is comparable with maximum of N_2O mixing ratios in early summer as observed at

515 Jungfraujoch (Fig. 1c). This underlines the importance of soil emission in accounting for
516 atmospheric N_2O variability (Saikawa et al., 2014). In late summer, the minimum of $\delta^{15}N^{SP}$ (Fig.
517 3) may be then attributed to the influence of soil emitted N_2O, which has lower $\delta^{15}N^{SP}$ (7.2±3.8‰;
518 Table 1) than the troposphere (Fig. 2). However, the STE process, which resulted in the minimum
519 of N_2O mixing ratio, likely contributes a positive isotope effect in the meanwhile (Kaiser et al.,
520 2006). In order to evaluate the combined effect of STE and soil emission on $\delta^{15}N^{SP}$ in late summer,
521 we applied a mixing calculation. Such estimate was made based on the approximated N_2O
522 enhancement/depletion contributed by the two processes and the assumed isotope effects (see more
523 details in M&M). The mixing calculation indicated an overall isotope effect of about 0.01‰, which
524 is extremely small and below our analytic precision. This practice suggests that it is still
525 challenging to build a direct link between N_2O sources/processes and the observed isotope
526 signature in the background atmosphere. It is also noteworthy that the $\delta^{15}N^{SP}$ used in the
527 calculation (7.2±3.8‰) may underestimate the isotope effects of soil emission, given that
528 denitrification, as a major N_2O process in soils, produces N_2O with $\delta^{15}N^{SP}$ close to 0‰ (Sutka et
529 al., 2006). Previous field studies have demonstrated that low-$\delta^{15}N^{SP}$ N_2O emissions (~0‰), i.e.
530 following the denitrification pathway, predominates during summer periods at Swiss (Wolf et al.,
531 2015) and German (Ibraim et al., 2019) grasslands. By contrast, the influence of biogeochemical
532 processes (nitrification and denitrification) on $\delta^{15}N^{bulk}$ is generally smaller than that on $\delta^{15}N^{SP}$
533 (Toyoda et al., 2011), and such effect on $\delta^{15}N^{bulk}$ are usually overwritten by the wide range of
534 isotopic signatures in soil N substrates (Sutka et al., 2006). Hence, given the distinct $\delta^{15}N^{bulk}$
535 maximum and N_2O minimum in late summer during our observation (Figs. 1 and 3), we suggest
536 that the STE process is mainly responsible for the seasonal variability in $\delta^{15}N^{bulk}$.

537 The footprint analyses based on air mass residence time revealed a seasonal pattern, with a higher

538 contribution of background air from the FT and SW regions in winter and more pronounced
539 contribution of local planetary boundary layer air from the L, E and NW regions in summer (Fig.
540 4b). The higher frequency of air mass footprints recently in contact with the surface in summer is
541 consistent with inverse modeling results, indicating a larger contribution of soil N_2O emissions in
542 June/July (Fig. 7). For the air mass regime representing the free troposphere, N_2O mixing ratios
543 observed at Jungfraujoch were significantly below the average, while $\delta^{15}N^{SP}$ and $\delta^{18}O$ were higher
544 (Fig. 6). By contrast, the local cluster (L) representing a strong impact from the planetary boundary
545 layer had higher N_2O mixing ratios and lower isotopic signatures (except $\delta^{15}N^{bulk}$) than the other
546 source regions. In addition, the ratio of NO_y to CO, which is a more straightforward indicator of
547 the free troposphere (Zellweger et al., 2003), show significant negative correlations with $\delta^{15}N^{SP}$
548 and $\delta^{18}O$, but not with $\delta^{15}N^{bulk}$ (Fig. 8). This further suggests that the seasonal variability of $\delta^{15}N^{SP}$
549 and $\delta^{18}O$ observed at Jungfraujoch is most likely influenced by ground-derived emissions, while
550 fluctuations in N_2O mixing ratios and $\delta^{15}N^{bulk}$ are possibly driven by STE.

551 Considering the complexity in mechanisms responsible for N_2O isotopic variations, we strongly
552 recommend more field measurements of N_2O isotopic signatures at higher frequency and at
553 different background sites, in order to cover spatial and temporal variability in N_2O sources. For
554 example, in the second phase, we only detected a significant seasonality of $\delta^{15}N^{SP}$, with a minimum
555 in July, which is one month earlier than the summer minimum found for the whole dataset (Fig.
556 3). This may be attributed to a difference in source regions, as Northwest regions appeared to be
557 significantly more important during 2017 (second phase). However, due to low sampling
558 frequency, it is challenging to overcome the large uncertainty in seasonality analysis for a two-
559 year period such as the second phase.

560 Based on our bottom-up approach, we simulated isotopic signatures for the overall N_2O sources

responsible for the N_2O mixing ratio increase in the atmosphere (Fig. 9). However, the interpretation of simulated versus observed variability in N_2O isotopic composition was difficult, except for the somewhat similar patterns in $\delta^{18}O$. Our results suggest a limitation in the current knowledge and literature values on isotopic signatures of most N_2O sources. In addition, most N_2O sources may not exhibit a well-defined isotopic signature but a range of values regulated under a number of processes/environmental factors. For example, isotopic signatures of soil-derived N_2O are often determined by an interaction of several soil and climatic factors. It might be possible in the future to model these changes implementing isotopes in ecosystem models, as recently demonstrated by Denk et al. (2019).

4.3 Interannual trends of atmospheric N_2O isotopic composition

Over a period of almost five years, our observations show an interannual increase in N_2O mixing ratio and decrease in $\delta^{15}N^{bulk}$ (Fig. 10). This is to be expected, assuming that the atmospheric N_2O increase is primarily attributed to anthropogenic sources, which emit isotopically lighter N_2O relative to the tropospheric background (Table 1) (Rahn and Wahlen, 2000). Compared to several studies on firn air (Ishijima et al., 2007; Röckmann et al., 2003) and surface air (Park et al., 2012; Röckmann and Levin, 2005; Toyoda et al., 2013), the rate of decrease for $\delta^{15}N^{bulk}$ at Jungfraujoch is relatively high (-0.05 to -0.06 ‰ a^{-1}, Table 3). Such a discrepancy in the $\delta^{15}N^{bulk}$ trend could be due to a large contribution of terrestrial N_2O emission from the European continent to Jungfraujoch (Figs. 6 and 7), as N_2O originating from soil emissions is significantly more isotopically depleted than that of oceanic sources (Snider et al., 2015b). Nevertheless, our observation period is shorter than that of other studies, so the interannual trends determined here are more likely affected by year-to-year variability. Among all reported records, the decrease of $\delta^{15}N^{bulk}$ observed at Hateruma Island was the most up-to-date and smallest (-0.020-0.026‰ a^{-1}) (Toyoda et al., 2013). The authors

584 argued that the smaller declining trend for $\delta^{15}N^{bulk}$ may be explained by the recent increase in
585 anthropogenic isotopic ratios particularly for agricultural N_2O emissions, although Ishijima et al.
586 (2007) suggested a decline in both $\delta^{15}N^{bulk}$ and $\delta^{18}O$ in anthropogenic N_2O from 1952-1970 to
587 1970-2001 based on inverse modeling.

588 For the interannual trends observed at Jungfraujoch, it is noteworthy to point out that our
589 observations covering a rather short period may lead to large uncertainties despite statistical
590 significance. The discrepancy found in the trends between the first and second phases indicates
591 that variability of N_2O isotopic composition is likely to obscure interannual trends over shorter
592 periods (Toyoda et al., 2013). Hence, extended time-series of isotopic measurements are needed
593 to reevaluate, for example, the observed tendency of increase in $\delta^{18}O$ and $\delta^{15}N^{SP}$ at Jungfraujoch
594 (Table 3; only significant during the first phase). For $\delta^{18}O$ of atmospheric N_2O, a generally
595 declining trend smaller than that of $\delta^{15}N^{bulk}$ has been indicated by a number of observations
596 (Bernard et al., 2006; Ishijima et al., 2007; Park et al., 2012; Röckmann et al., 2003; Röckmann
597 and Levin, 2005). This is expected as $\delta^{18}O$ of anthropogenic N_2O is not much different from that
598 of the natural background, assuming that the oxygen atom in N_2O is largely derived from soil water
599 and ambient oxygen during production (Rahn and Wahlen, 2000).

600 It is still a challenging task to disentangle interannual trends of $\delta^{15}N^{SP}$-N_2O in the background
601 atmosphere, due to limitations in analytical repeatability and precision (Harris et al., 2017; Mohn
602 et al., 2014). Past results have reached inconsistent conclusions, showing positive (Bernard et al.,
603 2006; Park et al., 2012; Prokopiou et al., 2017; Röckmann and Levin, 2005) or negative
604 (Röckmann et al., 2003; Toyoda et al., 2013) trends of similar magnitude (Fig. 10). On the one
605 hand, the negative trend in $\delta^{15}N^{SP}$ could be explained by the significantly lower $\delta^{15}N^{SP}$ from
606 anthropogenic sources (e.g. agricultural sources; Table 1) than of the tropospheric background

607 (near 18‰; Fig. 10). On the other hand, Park et al. (2012) suggested that the increase of $\delta^{15}N^{SP}$ in
608 the atmospheric N_2O may reflect a global increase in importance of the contribution by nitrification
609 (high- $\delta^{15}N^{SP}$ process) to agricultural N_2O emissions. This is based on the assumption that the
610 growth of N_2O emissions is largely due to enhanced fertilizer application which promotes
611 nitrification activity (Pérez et al., 2001; Tian et al., 2019). The observed mean increase rate of 0.02‰
612 a^{-1} for $\delta^{15}N^{SP}$ by Park et al. (2012) could then be translated into an increase of 13-23% for the
613 relative amount of nitrification-derived N_2O between 1750 and 2005. However, this should be
614 further evaluated with more frequent sampling (Park et al. (2012) only sampled 1-6 times per year)
615 and tested with isotopic measurements across the NH, where agricultural N_2O emissions are more
616 dominant than in the SH. In addition, the strong seasonal pattern of $\delta^{15}N^{SP}$ at Jungfraujoch suggests
617 that seasonal variations of $\delta^{15}N^{SP}$ in response to climatic or source factors are crucial and must be
618 taken into consideration for evaluating interannual $\delta^{15}N^{SP}$ trends.

619 **4.4 Simulated anthropogenic N_2O sources with the two-box model and comparison with**
620 **other studies**

621 To further evaluate anthropogenic source signatures of N_2O isotopic composition, we applied a
622 two-box model representing a well-mixed troposphere and stratosphere (Röckmann et al., 2003;
623 Schilt et al., 2014; Sowers et al., 2002). The model runs with the whole dataset and the dataset
624 filtered for free-troposphere only (Table 4) exhibit statistically identical results, supporting that
625 our model estimates, with observations at Jungfraujoch, are representative of the background
626 atmosphere. The simulated trends of the N_2O mixing ratios and isotopic composition show a
627 gradual increase in N_2O and decrease in the isotopic signatures (see Fig. 10), which agree with
628 existing observations within the model uncertainty. However, this does not hold for individual
629 studies considered separately. For example, the N_2O mixing ratios observed by Röckmann et al.

630 (2003) and Prokopiou et al. (2017) would lead to a higher preindustrial N_2O compared to our
631 model simulation, which is likely due to the uncertainty in the firn air records (Prokopiou et al.,
632 2017).

633 We compared the anthropogenic isotopic signatures determined by our two-box model with other
634 similar studies in Table 4. Our estimates generally lie within the ranges given in the earlier studies
635 (Ishijima et al., 2007; Park et al., 2012; Prokopiou et al., 2017; Röckmann et al., 2003; Sowers et
636 al., 2002; Toyoda et al., 2013). However, isotopic signatures of N_2O sources estimated for 2018 in
637 this study are higher in $\delta^{15}N^{bulk}$ and $\delta^{18}O$ (by 4-8‰), and lower in $\delta^{15}N^{SP}$ (by 2-7‰) than model
638 estimates for the early 2000s from two other studies from SH (Park et al., 2012; Prokopiou et al.,
639 2017). Such differences in $\delta^{15}N^{bulk}$ and $\delta^{18}O$ could be related to interhemispheric differences, as
640 the relative contributions of N_2O sources vary between the two hemispheres (Toyoda et al., 2013).
641 Also, more interestingly, this could suggest a shift in the N_2O source isotopic signatures over the
642 last few decades. For example, an increase of $\delta^{15}N^{bulk}$ in anthropogenic N_2O sources over time
643 may be attributed to growing contributions of other industrial/waste sources with high $\delta^{15}N^{bulk}$
644 (Prokopiou et al., 2017). In addition, if the assumption of increasing $\delta^{15}N^{bulk}$ and decreasing $\delta^{15}N^{SP}$
645 in anthropogenic N_2O sources over time holds, it points to a recently growing contribution of
646 denitrification relative to nitrification, to the global atmospheric N_2O increase (Sutka et al., 2006;
647 Toyoda et al., 2013). By contrast, Park et al. (2012) and Prokopiou et al. (2017) proposed an
648 increasing importance of nitrification for anthropogenic N_2O emissions based on the increasing
649 $\delta^{15}N^{SP}$ trend since 1940. This may suggest that a strong climate change feedback has recently
650 resulted in significant shifts in N_2O source process, hence twisting the isotopic signatures of
651 anthropogenic sources (Griffis et al., 2017; Xu-Ri et al., 2012). Alternatively, the uncertainty in
652 determining N_2O isotopic signatures in the background atmosphere and inter-laboratory

653 comparability may play a role in the observed discrepancy.

654 Given the strong heterogeneity in source contributions to N_2O emissions around the globe
655 (Saikawa et al., 2014), current two- and four-box model estimates based on observations at
656 individual sites or regions are likely to reflect latitudinal or even interhemispheric differences in
657 anthropogenic isotopic signatures. On the other hand, previous discussions of the model
658 sensitivities by Röckmann et al. (2003) and Toyoda et al. (2013) have suggested that anthropogenic
659 isotopic values are most sensitive to the trends in tropospheric isotopic values and the relative
660 difference in tropospheric isotopic values between present and preindustrial times. For example,
661 given the similar parameters used for preindustrial times as our study, Park et al. (2012) observed
662 much lower $\delta^{15}N^{bulk}$ in the recent troposphere than in our case, hence resulting in significantly
663 lower $\delta^{15}N^{bulk}$ for the anthropogenic source. Furthermore, Park et al. (2012) and Prokopiou et al.
664 (2017) simulated a positive trend in $\delta^{15}N^{SP}$ relative to preindustrial times, which in return resulted
665 in a much higher $\delta^{15}N^{SP}$ for the anthropogenic sources.

666 Using an alternative bottom-up approach, we estimated the anthropogenic source isotopic
667 signatures based on the N_2O emission inventory simulated for Jungfraujoch and published source
668 isotopic signatures as summarized by Harris et al. (2017) (Table 1). The retrieved anthropogenic
669 isotopic signatures (Table 5) were largely in agreement with the isotopic signature of agricultural
670 soil emissions (Snider et al., 2015b; Wolf et al., 2015), indicating that this source could explain
671 more than 60% of the total N_2O emissions. However, the anthropogenic isotopic signatures
672 estimated by this approach were lower than the results from our two-box model (Table 4). In
673 contrast, another similar bottom-up estimate based on the global N_2O emission inventory (Toyoda
674 et al., 2013) reported anthropogenic isotopic values that agree well with our box-model results.
675 This may be explained by the different isotopic signatures used to describe agricultural N_2O

676 emissions, as those values used for the bottom-up estimates by Toyoda et al. (2013) were
677 significantly lower (Toyoda et al., 2011) than those used in this study (Snider et al., 2015b; Wolf
678 et al., 2015). Such bottom-up estimation suggests that more isotopic measurements of the
679 background atmosphere from different regions, and better constraints on individual anthropogenic
680 (especially agricultural) N_2O isotopic signatures, are necessary for a better representation of N_2O
681 isotopic composition in atmospheric modeling studies.

5 Conclusions

With the recently developed laser spectroscopic technique coupled with a preconcentration device, we achieved good repeatability in measurements of N_2O isotopic composition from the background atmosphere at Jungfraujoch, Switzerland. This time-series covered a period of five years and showed a distinct seasonality, with $\delta^{15}N^{bulk}$ maxima and $\delta^{15}N^{SP}$ minima in late summer, associated with the lowest N_2O mixing ratios over the year. The seasonal fluctuation of $\delta^{15}N^{bulk}$ was associated with the stratosphere-troposphere exchange process, in agreement with other monitoring networks (Nevison et al., 2011), while the contrasting depletion of $\delta^{15}N^{SP}$ in later summer is possibly a combined result of STE and agricultural emissions, with the latter being more important. The analyses of air mass transport regimes together with the simulation of N_2O enhancements for Jungfraujoch supported our explanations and highlighted that the fluctuation between the free troposphere and local contributions dominated by soil emission drives the seasonality of $\delta^{15}N^{SP}$ and $\delta^{18}O$ as observed at Jungfraujoch.

We found statistically significant interannual trends for $\delta^{15}N^{bulk}$, which is expected as anthropogenic N_2O sources are characterized by low ^{15}N abundance. For $\delta^{15}N^{SP}$ and $\delta^{18}O$, interannual trends were highly uncertain and possibly masked by their large temporal variabilities. Using a two-box model approach, we simulated the evolution of N_2O isotopic composition from preindustrial times to the present. This model suggests an overall decreasing trend for all isotopic deltas in conjunction with the atmospheric N_2O increase. The anthropogenic source signatures given by the model generally agreed with previous studies. However, these model results are still sensitive to the ranges and trends of the observed N_2O isotopic signatures in the present troposphere. In the future, more extended records of high-precision N_2O isotopic measurements

704 and application of multiple-box modeling approaches (Rigby et al., 2013) are necessary to account
705 for the global N_2O budget and evolution of anthropogenic sources.

Data availability

Data for this study have been deposited in a general data repository (https://figshare.com/s/077562ab408dd1bd0880; doi:10.6084/m9.figshare.12032760.v1, 2020).

Author contribution:

LY, EH and JM led and designed this study. LY, EH, SE conducted sample collection at Jungfraujoch; LY and EH analyzed discrete samples at Empa; MS and CZ contributed *in situ* measurements of N_2O, NO_y, CO and O_3 at Jungfraujoch; LY, EH and SH performed data analyses for the time-series and conducted model simulations. LY wrote the main manuscript; EH, SH and JM were involved in the revisions of the manuscript and commenting. SE, MS, LE and CZ were also involved in scientific discussion and commenting on the manuscript.

Competing interests

The authors declare that they have no conflict of interest.

Acknowledgements

We are thankful to the research infrastructure provided by the High Altitude Research Stations Jungfraujoch and Gornergrat. We are grateful to the help from the custodians (Mr. and Mrs. Fischer and Mr. and Mrs. Käser) at the research station of Jungfraujoch. We would like to thank Simon Wyss, Kerstin Zeyer, Patrik Zanchetta and Flurin Dietz for their support with the sample collection as well as laboratory assistance. The NABEL network is operated by Empa in collaboration with the Swiss Federal Office for the Environment. Prof. Sakae Toyoda and Prof. Naohiro Yoshida from Tokyo Institute of Technology are acknowledged for their analyses of the applied reference standards. This study was financially supported by the Swiss National Science Foundation (grant number 200021_163075) and the Swiss contribution to the Integrated Carbon Observation System

(ICOS) Research Infrastructure (ICOS-CH). ICOS-CH is funded by the Swiss National Science Foundation and in-house contributions. Longfei Yu was additionally supported by the EMPAPOSTDOCS-II program, which receives funding from the European Union's Horizon 2020 research and innovation program under the Marie Skłodowska-Curie grant agreement number 754364.

References

Appenzeller, C., Begert, M., Zenklusen, E. and Scherrer, S. C.: Monitoring climate at Jungfraujoch in the high Swiss Alpine region, Sci. Total Environ., 391(2–3), 262–268, doi:10.1016/j.scitotenv.2007.10.005, 2008.

Bernard, S., Röckmann, T., Kaiser, J., Barnola, J.-M., Fischer, H., Blunier, T. and Chappellaz, J.: Constraints on N_2O budget changes since pre-industrial time from new firn air and ice core isotope measurements, Atmos. Chem. Phys. Discuss., 5(4), 7547–7575, doi:10.5194/acpd-5-7547-2005, 2006.

Bourbonnais, A., Letscher, R. T., Bange, H. W., Échevin, V., Larkum, J., Mohn, J., Yoshida, N. and Altabet, M. A.: N_2O production and consumption from stable isotopic and concentration data in the Peruvian coastal upwelling system, Global Biogeochem. Cycles, 31(4), 678–698, doi:10.1002/2016GB005567, 2017.

Buchmann, B., Hueglin, C., Reimann, S., Vollmer, M. K., Steinbacher, M. and Emmenegger, L.: Reactive gases, ozone depleting substances and greenhouse gases, in From weather observations to atmospheric and climate sciences in Switzerland, edited by S. Willemse and M. Furger, vdf Hochschulverlag AG., 2016.

Bukowiecki, N., Weingartner, E., Gysel, M., Coen, M. C., Zieger, P., Herrmann, E., Steinbacher, M., Gäggeler, H. W. and Baltensperger, U.: A review of more than 20 years of aerosol observation at the high altitude research station Jungfraujoch, Switzerland (3580 m asl), Aerosol Air Qual. Res., 16(3), 764–788, doi:10.4209/aaqr.2015.05.0305, 2016.

Butterbach-Bahl, K., Baggs, E. M., Dannenmann, M., Kiese, R. and Zechmeister-Boltenstern, S.: Nitrous oxide emissions from soils: how well do we understand the processes and their controls?, Philos. Trans. R. Soc. Lond. B. Biol. Sci., 368, 20130122, doi:10.1098/rstb.2013.0122, 2013.

Decock, C. and Six, J.: How reliable is the intramolecular distribution of ^{15}N in N_2O to source partition N_2O emitted from soil?, Soil Biol. Biochem., 65(2), 114–127, doi:10.1016/j.soilbio.2013.05.012, 2013.

Denk, T. R. A., Mohn, J., Decock, C., Lewicka-Szczebak, D., Harris, E., Butterbach-Bahl, K., Kiese, R. and Wolf, B.: The nitrogen cycle: A review of isotope effects and isotope modeling approaches, Soil Biol. Biochem., 105, 121–137, doi:10.1016/j.soilbio.2016.11.015, 2017.

Denk, T. R. A., Kraus, D., Kiese, R., Butterbach-Bahl, K. and Wolf, B.: Constraining N cycling in the ecosystem model LandscapeDNDC with the stable isotope model SIMONE, Ecology, 100(5), c02675, doi:10.1002/ecy.2675, 2019.

Fowler, D., Steadman, C. E., Stevenson, D., Coyle, M., Rees, R. M., Skiba, U. M., Sutton, M. a., Cape, J. N., Dore, a. J., Vieno, M., Simpson, D., Zaehle, S., Stocker, B. D., Rinaldi, M., Facchini, M. C., Flechard, C. R., Nemitz, E., Twigg, M., Erisman, J. W. and Galloway, J. N.: Effects of global change during the 21st century on the nitrogen cycle, Atmos. Chem. Phys. Discuss., 15(2), 1747–1868, doi:10.5194/acpd-15-1747-2015, 2015.

Fujii, A., Toyoda, S., Yoshida, O., Watanabe, S., Sasaki, K. and Yoshida, N.: Distribution of nitrous oxide dissolved in water masses in the eastern subtropical North Pacific and its origin inferred from isotopomer analysis, J. Oceanogr., 69(2), 147–157, doi:10.1007/s10872-012-0162-4, 2013.

Griffis, T. J., Chen, Z., Baker, J. M., Wood, J. D., Millet, D. B., Lee, X., Venterea, R. T. and Turner, P. A.: Nitrous oxide emissions are enhanced in a warmer and wetter world, Proc. Natl. Acad. Sci., 201704552, doi:10.1073/pnas.1704552114, 2017.

Hall, B. D., Dutton, G. S. and Elkins, J. W.: The NOAA nitrous oxide standard scale for atmospheric observations, J. Geophys. Res. Atmos., 112(9), 1–9, doi:10.1029/2006JD007954, 2007.

776 Harris, E. J., Nelson, D. D., Olsewski, W., Zahniser, M., Potter, E., Mcmanus, B. J., Whitehill, A., Prinn,
777 R. G., Ono, S. and Harris, E.: Development of a spectroscopic technique for continuous online monitoring
778 of oxygen and site-specific nitrogen isotopic com, Anal. Chem., 86(3), 1726–1734, 2014.

779 Harris, E., Zeyer, K., Kegel, R., Müller, B., Emmenegger, L. and Mohn, J.: Nitrous oxide and methane
780 emissions and nitrous oxide isotopic composition from waste incineration in Switzerland, Waste Manag.,
781 35(x), 135–140, doi:10.1016/j.wasman.2014.10.016, 2015.

782 Harris, E., Ibraim, E., Henne, S., Hüglin, C., Zellweger, C., Tuzson, B., Emmenegger, L. and Mohn, J.:
783 Tracking nitrous oxide emission processes at a suburban site with semicontinuous , in situ measurements
784 of isotopic composition, J. Geophys. Res. Atmos., 122, 1850–1870, doi:10.1002/2016JD025906, 2017.

785 Heil, J., Wolf, B., Brüggemann, N., Emmenegger, L., Tuzson, B., Vereecken, H. and Mohn, J.: Site-
786 specific 15N isotopic signatures of abiotically produced N_2O, Geochim. Cosmochim. Acta, 139, 72–82,
787 doi:10.1016/j.gca.2014.04.037, 2014.

788 Henne, S., Brunner, D., Folini, D., Solberg, S., Klausen, J. and Buchmann, B.: Assessment of parameters
789 describing representativeness of air quality in-situ measurement sites, Atmos. Chem. Phys., 10(8), 3561–
790 3581, doi:10.5194/acp-10-3561-2010, 2010.

791 Henne, S., Brunner, D., Oney, B., Leuenberger, M., Eugster, W., Bamberger, I., Meinhardt, F.,
792 Steinbacher, M. and Emmenegger, L.: Validation of the Swiss methane emission inventory by
793 atmospheric observations and inverse modelling, Atmos. Chem. Phys., 16(6), 3683–3710,
794 doi:10.5194/acp-16-3683-2016, 2016.

795 Henne, S., Mohn, J. and Brunner, D.: Quantification of Swiss nitrous oxide emissions through
796 atmospheric observations and inverse modelling, Final Report, Project of FOEN, 2019.

797 Herrmann, E., Weingartner, E., Henne, S., Vuilleumier, L., Bukowiecki, N., Steinbacher, M., Conen, F.,
798 Coen, M. C., Hammer, E., Juranyi, Z., Baltensperger, U. and Gysel, M.: Analysis of long-term aerosol
799 size distribution data from Jungfraujoch with emphasis on free tropospheric conditions, cloud influence,
800 and air mass transport, J. Geophys. Res. Atmos., 120, 1751–1762, doi:10.1002/2015JD023660, 2015.

801 Ibraim, E., Wolf, B., Harris, E., Gasche, R., Wei, J., Yu, L., Kiese, R., Eggleston, S., Butterbach-Bahl, K.,
802 Zeeman, M., Tuzson, B., Emmenegger, L., Six, J., Henne, S. and Mohn, J.: Attribution of N_2O sources in
803 a grassland soil with laser spectroscopy based isotopocule analysis, Biogeosciences, 16, 3247–3266,
804 doi.org/10.5194/bg-16-3247-2019, 2019.

805 Ishijima, K., Sugawara, S., Kawamura, K., Hashida, G., Morimoto, S., Murayama, S., Aoki, S. and
806 Nakazawa, T.: Temporal variations of the atmospheric nitrous oxide concentration and its $\delta^{15}N$ and $\delta^{18}O$
807 for the latter half of the 20th century reconstructed from firn air analyses, J. Geophys. Res. Atmos.,
808 112(3), doi:10.1029/2006JD007208, 2007.

809 Janssens-Maenhout, G., Crippa, M., Guizzardi, D., Muntean, M., Schaaf, E., Dentener, F., Bergamaschi,
810 P., Pagliari, V., Olivier, J., Peters, J., van Aardenne, J., Monni, S., Doering, U., Petrescu, R., Solazzo, E.
811 and Oreggioni, G.: EDGAR v4.3.2 Global Atlas of the three major Greenhouse Gas Emissions for the
812 period 1970-2012, Earth Syst. Sci. Data Discuss., 2010, 1–52, doi:10.5194/essd-2018-164, 2019.

813 Jiang, X., Ku, W. L., Shia, R. L., Li, Q., Elkins, J. W., Prinn, R. G. and Yung, Y. L.: Seasonal cycle of
814 N_2O: Analysis of data, Global Biogeochem. Cycles, 21, GB1006, doi:10.1029/2006GB002691, 2007.

815 JMA and WMO: World Meteorological Organization - Global Atmosphere Watch - World Data Centre
816 for Greenhouse Gases, Data Summary, No. 42, 101 p.,. [online] Available from:
817 https://gaw.kishou.go.jp/static/publications/summary/sum42/sum42.pdf, 2018.

818 Kaiser, J., Röckmann, T. and Brenninkmeijer, C. A. M.: Complete and accurate mass spectrometric
819 isotope analysis of tropospheric nitrous oxide, J. Geophys. Res. Atmos., 108, 4476,

820 doi:10.1029/2003JD003613, D15, 2003.

821 Kaiser, J., Engel, A., Borchers, R. and Röckmann, T.: Probing stratospheric transport and chemistry with
822 new balloon and aircraft observations of the meridional and vertical N_2O isotope distribution, Atmos.
823 Chem. Phys., 6(11), 3535–3556, doi:10.5194/acp-6-3535-2006, 2006.

824 Keller, C. A., Hill, M., Vollmer, M. K., Henne, S., Brunner, D., Reimann, S., O'Doherty, S., Arduini, J.,
825 Maione, M., Ferenczi, Z., Haszpra, L., Manning, A. J. and Peter, T.: European emissions of halogenated
826 greenhouse gases inferred from atmospheric measurements, Environ. Sci. Technol., 46(1), 217–225,
827 doi:10.1021/es202453j, 2012.

828 Kim, K.-R. and Craig, H.: Nitrogen-15 and Oxygen-18 Characacteristics of Nitrous Oxide: A Global
829 Perspective, Science , 262, 1855-1857, 1993.

830 Lebegue, B., Schmidt, M., Ramonet, M., Wastine, B., Yver Kwok, C., Laurent, O., Belviso, S., Guemri,
831 A., Philippon, C., Smith, J. and Conil, S.: Comparison of nitrous oxide (N_2O) analyzers for high-precision
832 measurements of atmospheric mole fractions, Atmos. Meas. Tech., 9(3), 1221–1238, doi:10.5194/amt-9-
833 1221-2016, 2016.

834 Logan, J. A., Staehelin, J., Megretskaia, I. A., Cammas, J. P., Thouret, V., Claude, H., De Backer, H.,
835 Steinbacher, M., Scheel, H. E., Stbi, R., Frhlich, M. and Derwent, R.: Changes in ozone over Europe:
836 Analysis of ozone measurements from sondes, regular aircraft (MOZAIC) and alpine surface sites, J.
837 Geophys. Res. Atmos., 117(9), 1–23, doi:10.1029/2011JD016952, 2012.

838 Maeda, K., Toyoda, S., Shimojima, R., Osada, T., Hanajima, D., Morioka, R. and Yoshida, N.: Source of
839 nitrous oxide emissions during the cow manure composting process as revealed by isotopomer analysis of
840 and amoa abundance in betaproteobacterial ammonia-oxidizing bacteria, Appl. Environ. Microbiol.,
841 76(5), 1555–1562, doi:10.1128/AEM.01394-09, 2010.

842 Mohn, J., Guggenheim, C., Tuzson, B., Vollmer, M. K., Toyoda, S., Yoshida, N. and Emmenegger, L.: A
843 liquid nitrogen-free preconcentration unit for measurements of ambient N_2O isotopomers by QCLAS,
844 Atmos. Meas. Tech., 3(3), 609–618, doi:10.5194/amt-3-609-2010, 2010.

845 Mohn, J., Tuzson, B., Manninen, A., Yoshida, N., Toyoda, S., Brand, W. A. and Emmenegger, L.: Site
846 selective real-time measurements of atmospheric N2O isotopomers by laser spectroscopy, Atmos. Meas.
847 Tech., 5(7), 1601–1609, doi:10.5194/amt-5-1601-2012, 2012.

848 Mohn, J., Wolf, B., Toyoda, S., Lin, C. T., Liang, M. C., Brüggemann, N., Wissel, H., Steiker, A. E.,
849 Dyckmans, J., Szwec, L., Ostrom, N. E., Casciotti, K. L., Forbes, M., Giesemann, A., Well, R., Doucett,
850 R. R., Yarnes, C. T., Ridley, A. R., Kaiser, J. and Yoshida, N.: Interlaboratory assessment of nitrous
851 oxide isotopomer analysis by isotope ratio mass spectrometry and laser spectroscopy: Current status and
852 perspectives, Rapid Commun. Mass Spectrom., 28(18), 1995–2007, doi:10.1002/rcm.6982, 2014.

853 Nevison, C. D., Keeling, R. F., Weiss, R. F., Popp, B. N., Jin, X., Fraser, P. J., Porter, L. W. and Hess, P.
854 G.: Southern Ocean ventilation inferred from seasonal cycles of atmospehric N_2O and O_2/N_2 at Cape
855 Grim, Tasmania, Tellus, Ser. B Chem. Phys. Meteorol., 57(3), 218–229, doi:10.1111/j.1600-
856 0889.2005.00143.x, 2005.

857 Nevison, C. D., Dlugokencky, E., Dutton, G., Elkins, J. W., Fraser, P., Hall, B., Krummel, P. B.,
858 Langenfelds, R. L., O'Doherty, S., Prinn, R. G., Steele, L. P. and Weiss, R. F.: Exploring causes of
859 interannual variability in the seasonal cycles of tropospheric nitrous oxide, Atmos. Chem. Phys., 11(8),
860 3713–3730, doi:10.5194/acp-11-3713-2011, 2011.

861 Ogawa, M. and Yoshida, N.: Intramolecular distribution of stable nitrogen and oxygen isotopes of nitrous
862 oxide emitted during coal combustion, Chemosphere, 61(6), 877–887,
863 doi:10.1016/j.chemosphere.2005.04.096, 2005a.

864 Ogawa, M. and Yoshida, N.: Nitrous oxide emission from the burning of agricultural residue, Atmos.

Environ., 39(19), 3421–3429, doi:10.1016/j.atmosenv.2005.01.059, 2005b.

Ostrom, N. E., Gandhi, H., Coplen, T. B., Toyoda, S., Böhlke, J. K., Brand, W. A., Casciotti, K. L., Dyckmans, J., Giesemann, A., Mohn, J., Well, R., Yu, L. and Yoshida, N.: Preliminary assessment of stable nitrogen and oxygen isotopic composition of USGS51 and USGS52 nitrous oxide reference gases and perspectives on calibration needs, Rapid Commun. Mass Spectrom., 32(15), 1207–1214, doi:10.1002/rcm.8157, 2018.

Pandey Deolal, S., Brunner, D., Steinbacher, M., Weers, U. and Staehelin, J.: Long-term in situ measurements of NO_x and NO_y at Jungfraujoch 1998-2009: Time series analysis and evaluation, Atmos. Chem. Phys., 12(5), 2551–2566, doi:10.5194/acp-12-2551-2012, 2012.

Park, S., Croteau, P., Boering, K. A., Etheridge, D. M., Ferretti, D., Fraser, P. J., Kim, K.-R., Krummel, P. B., Langenfelds, R. L., van Ommen, T. D., Steele, L. P. and Trudinger, C. M.: Trends and seasonal cycles in the isotopic composition of nitrous oxide since 1940, Nat. Geosci., 5(4), 261–265, doi:10.1038/ngeo1421, 2012.

Pérez, T., Trumbore, S. E., Tyler, S. C., Matson, P. A., I., O.-M., Rahn, T. and Griffiths, D. W. T.: Identifying the agricultural imprint on the global N2O budget using stable isotopes, J. Geophys. Res., 106, 9869–9878, doi:10.1179/1607845413y.0000000087, 2001.

Prather, M. J., Hsu, J., Deluca, N. M., Jackman, C. H., Oman, L. D., Douglass, A. R., Fleming, E. L., Strahan, S. E., Steenrod, S. D., Søvde, O. A., Isaksen, I. S. A., Froidevaux, L. and Funke, B.: Measuring and modeling the lifetime of nitrous oxide including its variability Michael, J. Geophys. Res. Atmos., 120, 5693–5705, doi:10.1002/2015JD023267.Received, 2015.

Prinn, R. G., Weiss, R. F., Arduini, J., Arnold, T., Dewitt, H. L., Fraser, P. J., Ganesan, A. L., Gasore, J., Harth, C. M., Hermansen, O., Kim, J., Krummel, P. B., Li, S., Loh, Z. M., Lunder, C. R. and Maione, M.: History of chemically and radiatively important atmospheric gases from the Advanced Global Atmospheric Gases Experiment (AGAGE), Earth Syst. Sci. Data, 10, 985–1018, 2018.

Prokopiou, M., Martinerie, P., Sapart, C. J., Witrant, E., Monteil, G. A., Ishijima, K., Bernard, S., Kaiser, J., Levin, I., Sowers, T., Blunier, T., Etheridge, D., Dlugokencky, E., van de Wal, R. S. W. and Röckmann, T.: Constraining N_2O emissions since 1940 using firn air isotope measurements in both hemispheres, Atmos. Chem. Phys., 2011(June), 1–50, doi:10.5194/acp-2016-487, 2017.

Prokopiou, M., Sapart, C. J., Rosen, J., Sperlich, P., Blunier, T., Brook, E., van de Wal, R. S. W. and Röckmann, T.: Changes in the Isotopic Signature of Atmospheric Nitrous Oxide and Its Global Average Source During the Last Three Millennia, J. Geophys. Res. Atmos., 1–17, doi:10.1029/2018JD029008, 2018.

Rahn, T. and Wahlen, M.: A reassessment of the global isotopic budget of atmospheric nitrous oxide, Global Biogeochem. Cycles, 14(2), 537–543, doi:10.1029/1999GB900070, 2000.

Ravishankara, A. R., Daniel, J. S. and Portmann, R. W.: Nitrous oxide (N_2O): the dominant ozone-depleting substance emitted in the 21st century., Science, 326(5949), 123–5, doi:10.1126/science.1176985, 2009.

Reay, D. S., Davidson, E. a., Smith, K. a., Smith, P., Melillo, J. M., Dentener, F. and Crutzen, P. J.: Global agriculture and nitrous oxide emissions, Nat. Clim. Chang., 2(6), 410–416, doi:10.1038/nclimate1458, 2012.

Reimann, S., Vollmer, M. K., Folini, D., Steinbacher, M., Hill, M., Buchmann, B., Zander, R. and Mahieu, E.: Observations of long-lived anthropogenic halocarbons at the high-Alpine site of Jungfraujoch (Switzerland) for assessment of trends and European sources, Sci. Total Environ., 391(2–3), 224–231, doi:10.1016/j.scitotenv.2007.10.022, 2008.

Rigby, M., Prinn, R. G., O'Doherty, S., Montzka, S. A., McCulloch, A., Harth, C. M., Mühle, J.,

910 Salameh, P. K., Weiss, R. F., Young, D., Simmonds, P. G., Hall, B. D., Dutton, G. S., Nance, D.,
911 Mondeel, D. J., Elkins, J. W., Krummel, P. B., Steele, L. P. and Fraser, P. J.: Re-evaluation of the
912 lifetimes of the major CFCs and CH3CCl3 using atmospheric trends, Atmos. Chem. Phys., 13(5), 2691–
913 2702, doi:10.5194/acp-13-2691-2013, 2013.

914 Röckmann, T., Kaiser, J. and Brenninkmeijer, C. A. M.: The isotopic fingerprint of the pre-industrial and
915 the anthropogenic N_2O source, Atmos. Chem. Phys., (3), 315–323, 2003.

916 Röckmann, T. and Levin, I.: High-precision determination of the changing isotopic composition of
917 atmospheric N_2O from 1990 to 2002, J. Geophys. Res. Atmos., 110(21), 1–8,
918 doi:10.1029/2005JD006066, 2005.

919 Saikawa, E., Prinn, R. G., Dlugokencky, E., Ishijima, K., Dutton, G. S., Hall, B. D., Langenfelds, R.,
920 Tohjima, Y., Machida, T., Manizza, M., Rigby, M., O'Doherty, S., Patra, P. K., Harth, C. M., Weiss, R.
921 F., Krummel, P. B., Van Der Schoot, M., Fraser, P. J., Steele, L. P., Aoki, S., Nakazawa, T. and Elkins, J.
922 W.: Global and regional emissions estimates for N_2O, Atmos. Chem. Phys., 14(9), 4617–4641,
923 doi:10.5194/acp-14-4617-2014, 2014.

924 Schibig, M. F., Steinbacher, M., Buchmann, B., Van Der Laan-Luijkx, I. T., Van Der Laan, S., Ranjan, S.
925 and Leuenberger, M. C.: Comparison of continuous in situ CO_2 observations at Jungfraujoch using two
926 different measurement techniques, Atmos. Meas. Tech., 8(1), 57–68, doi:10.5194/amt-8-57-2015, 2015.

927 Schilt, A., Brook, E. J., Bauska, T. K., Baggenstos, D., Fischer, H., Joos, F., Petrenko, V. V., Schaefer,
928 H., Schmitt, J., Severinghaus, J. P., Spahni, R. and Stocker, T. F.: Isotopic constraints on marine and
929 terrestrial N_2O emissions during the last deglaciation, Nature, 516(7530), 234–237,
930 doi:10.1038/nature13971, 2014.

931 Sepúlveda, E., Schneider, M., Hase, F., Barthlott, S., Dubravica, D., García, O. E., Gomez-Pelaez, A.,
932 González, Y., Guerra, J.C., Gisi, M., Kohlhepp, R., Dohe, S., Blumenstock, T., Strong, K., Weaver, D.,
933 Palm, N., Sadeghi, A., Deutscher, N. M., Warneke, T., Notholt, J., Jones, N., Griffith, D. W. T., Smale,
934 D., Brailsford, G. W., Robinson, J., Meinhardt, F., Steinbacher, M., Aalto, T. and Worthy, D.:
935 Tropospheric CH_4 signals as observed by NDACC FTIR at globally distributed sites and comparison to
936 GAW surface in situ measurements, Atmos. Meas. Tech., 7(7), 2337–2360, doi:10.5194/amt-7-2337-
937 2014, 2014.

938 Snider, D., Thompson, K., Wagner-Riddle, C., Spoelstra, J. and Dunfield, K.: Molecular techniques and
939 stable isotope ratios at natural abundance give complementary inferences about N_2O production pathways
940 in an agricultural soil following a rainfall event, Soil Biol. Biochem., 88, 197–213,
941 doi:10.1016/j.soilbio.2015.05.021, 2015a.

942 Snider, D. M., Venkiteswaran, J. J., Schiff, S. L. and Spoelstra, J.: From the ground up: Global nitrous
943 oxide sources are constrained by stable isotope values, PLoS One, 10(3), 1–19,
944 doi:10.1371/journal.pone.0118954, 2015b.

945 Sowers, T., Rodebaugh, A., Yoshida, N. and Toyoda, S.: Extending records of the isotopic composition of
946 atmospheric N_2O back to 1800 A.D. from air trapped in snow at the South Pole and the Greenland Ice
947 Sheet Project II ice core, Global Biogeochem. Cycles, 16(4), 1–10, doi:10.1029/2002GB001911, 2002.

948 Stohl, A., Forster, C., Frank, A., Seibert, P. and Wotawa, G.: Technical note: The Lagrangian particle
949 dispersion model FLEXPART version 6.2, Atmos. Chem. Phys., 5, 2461–2474,
950 doi:10.3390/atmos9020076, 2005.

951 Sturm, P., Tuzson, B., Henne, S. and Emmenegger, L.: Tracking isotopic signatures of CO_2 at the high
952 altitude site Jungfraujoch with laser spectroscopy: Analytical improvements and representative results,
953 Atmos. Meas. Tech., 6(7), 1659–1671, doi:10.5194/amt-6-1659-2013, 2013.

954 Sutka, R. L., Ostrom, N. E., Ostrom, P. H., Breznak, J. a, Pitt, a J., Li, F. and Gandhi, H.: Distinguishing

Nitrous Oxide Production from Nitrification and Denitrification on the Basis of Isotopomer Abundances Distinguishing Nitrous Oxide Production from Nitrification and Denitrification on the Basis of Isotopomer Abundances, Appl. Environ. Microbiol., 72(1), 638–644, doi:10.1128/AEM.72.1.638, 2006.

Tarasova, O. A., Senik, I. A., Sosonkin, M. G., Cui, J., Staehelin, J. and Péevôt, A. S. H.: Surface ozone at the Caucasian site Kislovodsk High Mountain Station and the Swiss Alpine site Jungfraujoch: Data analysis and trends (1990-2006), Atmos. Chem. Phys., 9(12), 4157–4175, doi:10.5194/acp-9-4157-2009, 2009.

Team, R. C.: A language and environment for statistical computing. R Foundation for statistical computing, 2015; Vienna, Austria, 2016.

Thiemens, M. H. and Trogler, W. C.: Nylon Production: An Unknown Source of Atmospheric Nitrous Oxide, Science, 251(4996), 932–934, doi:10.1126/science.251.4996.932, 1991.

Thompson, R. L., Patra, P. K., Ishijima, K., Saikawa, E., Corazza, M., Karstens, U., Wilson, C., Bergamaschi, P., Dlugokencky, E., Sweeney, C., Prinn, R. G., Weiss, R. F., O'Doherty, S., Fraser, P. J., Steele, L. P., Krummel, P. B., Saunois, M., Chipperfield, M. and Bousquet, P.: TransCom N_2O model inter-comparison-Part 1: Assessing the influence of transport and surface fluxes on tropospheric N_2O variability, Atmos. Chem. Phys., 14(8), 4349–4368, doi:10.5194/acp-14-4349-2014, 2014a.

Thompson, R. L., Ishijima, K., Saikawa, E., Corazza, M., Karstens, U., Patra, P. K., Bergamaschi, P., Chevallier, F., Dlugokencky, E., Prinn, R. G., Weiss, R. F., O'Doherty, S., Fraser, P. J., Steele, L. P., Krummel, P. B., Vermeulen, A., Tohjima, Y., Jordan, A., Haszpra, L., Steinbacher, M., Van Der Laan, S., Aalto, T., Meinhardt, F., Popa, M. E., Moncrieff, J. and Bousquet, P.: TransCom N_2O model inter-comparison - Part 2: Atmospheric inversion estimates of N_2O emissions, Atmos. Chem. Phys., 14(12), 6177–6194, doi:10.5194/acp-14-6177-2014, 2014b.

Thoning, K. W., Tans, P. P. and Komhyr, W. D.: Atmospheric carbon dioxide at Mauna Loa Observatory: 2. Analysis of the NOAA GMCC data, 1974-1985, J. Geophys. Res., 94(D6), 8549–8565, doi:10.1029/jd094id06p08549, 1989.

Tian, H., Yang, J., Xu, R., Lu, C., Canadell, J., Davidson, E. A., Jackson, R., Arneth, A., Chang, J., Ciais, P., Gerber, S., Ito, A., Joos, F., Lienert, S., Messina, P., Olin, S., Pan, S., Peng, C., Saikawa, E., Thompson, R., Vuichard, N., Winiwarter, W., Zaehle, S. and Zhang, B.: Global soil nitrous oxide emissions since the preindustrial era estimated by an ensemble of terrestrial biosphere models: Magnitude, attribution, and uncertainty, Glob. Chang. Biol., 25(2), 640–659, doi:10.1111/gcb.14514, 2019.

Toyoda, S., Yoshida, N., Urabe, T., Aoki, S., Nakazawa, T., Sugawara, S. and Honda, H.: Fractionation of N_2O isotopomers in the stratosphere, J. Geophys. Res., 106(D7), 7515, doi:10.1029/2000JD900680, 2001.

Toyoda, S., Yamamoto, S., Arai, S., Nara, H., Yoshida, N., Kashiwakura, K. and Akiyama, K.: Isotopomeric characterization of N2O produced, consumed, and emitted by automobiles, rapid comm, 22, 603–612, doi:10.1002/rcm, 2008.

Toyoda, S., Yano, M., Nishimura, S., Akiyama, H., Hayakawa, A., Koba, K., Sudo, S., Yagi, K., Makabe, A., Tobari, Y., Ogawa, N. O., Ohkouchi, N., Yamada, K. and Yoshida, N.: Characterization and production and consumption processes of N_2O emitted from temperate agricultural soils determined via isotopomer ratio analysis, Global Biogeochem. Cycles, 25(2), 1–17, doi:10.1029/2009GB003769, 2011.

Toyoda, S., Kuroki, N., Yoshida, N., Ishijima, K., Tohjima, Y. and Machida, T.: Decadal time series of tropospheric abundance of N_2O isotopomers and isotopologues in the Northern Hemisphere obtained by the long-term observation at Hateruma Island, Japan, J. Geophys. Res. Atmos., 118(8), 3369–3381, doi:10.1002/jgrd.50221, 2013.

Toyoda, S., Yoshida, N. and Koba, K.: Isotopocule analysis of biologically produced nitrous oxide in various environments, Mass Spectrom. Rev., (36), 135–160, doi:doi:10.1002/mas.21459, 2017.

Toyoda, S., Yoshida, N., Morimoto, S., Aoki, S., Nakazawa, T., Sugawara, S., Ishidoya, S., Uematsu, M., Inai, Y., Hasebe, F., Ikeda, C., Honda, H. and Ishijima, K.: Vertical distributions of N_2O isotopocules in the equatorial stratosphere, Atmos. Chem. Phys., (18), 833–844, 2018.

Tuzson, B., Henne, S., Brunner, D., Steinbacher, M., Mohn, J., Buchmann, B. and Emmenegger, L.: Continuous isotopic composition measurements of tropospheric CO_2 at Jungfraujoch (3580 m a.s.l.), Switzerland: Real-time observation of regional pollution events, Atmos. Chem. Phys., 11(4), 1685–1696, doi:10.5194/acp-11-1685-2011, 2011.

WMO: WMO Greenhouse Gas Bulletin., 2018.

Wolf, B., Merbold, L., Decock, C., Tuzson, B., Harris, E., Six, J., Emmenegger, L. and Mohn, J.: First on-line isotopic characterization of N2O above intensively managed grassland, Biogeosciences, 12(8), 2517–2531, doi:10.5194/bg-12-2517-2015, 2015.

Xu-Ri, Prentice, I. C., Spahni, R. and Niu, H. S.: Modelling terrestrial nitrous oxide emissions and implications for climate feedback, New Phytol., 196(2), 472–488, doi:10.1111/j.1469-8137.2012.04269.x, 2012.

Yoshida, N. and Toyoda, S.: Constraining the atmospheric N_2O budget from intramolecular site preference in N_2O isotopomers, Nature, 405(6784), 330–4, doi:10.1038/35012558, 2000.

Yuan, Y., Ries, L., Petermeier, H., Steinbacher, M., Gómez-Pelaéz, A. J., Leuenberger, M. C., Schumacher, M., Trickl, T., Couret, C., Meinhardt, F. and Menzel, A.: Adaptive selection of diurnal minimum variation: A statistical strategy to obtain representative atmospheric CO_2 data and its application to European elevated mountain stations, Atmos. Meas. Tech., 11(3), 1501–1514, doi:10.5194/amt-11-1501-2018, 2018.

Yung, Y. L. and Miller, C. E.: Isotopic fractionation of stratospheric nitrous oxide, Science, 278(5344), 1778–1780, doi:10.1126/science.278.5344.1778, 1997.

Zellweger, C., Forrer, J., Hofer, P., Nyeki, S., Schwarzenbach, B., Weingartner, E., Ammann, M. and Baltensperger, U.: Partitioning of reactive nitrogen (NO_y) and dependence on meteorological conditions in the lower free troposphere, Atmos. Chem. Phys., 3(3), 779–796, doi:10.5194/acp-3-779-2003, 2003.

Zellweger, C., Hüglin, C., Klausen, J., Steinbacher, M., Vollmer, M. and Buchmann, B.: Inter-comparison of four different carbon monoxide measurement techniques and evaluation of the long-term carbon monoxide time series of Jungfraujoch, Atmos. Chem. Phys., 9(11), 3491–3503, doi:10.5194/acp-9-3491-2009, 2009.

1032 **Table 1** An overview of N_2O emission sectors for Swiss Meteotest Inventory and global EDAGR Inventory and available source isotopic
1033 signatures (‰)*

Meteotest Category	Meteotest Source(s)	EDGAR Category$^{\varphi}$	EDGAR Primary source(s)$^{\varphi}$	$\delta^{18}O$	$\delta^{15}N^{bulk}$	$\delta^{15}N^{SP}$	References
Orgs	Organic soils	7B, 7C	Indirect soil emissions	29.0±3.7	-17.8±5.7	7.2±3.8	Snider et al. (2015b), Wolf et al. (2015)
IndustrialHeating	Cement production, industrial combustion, furnaces, waste incinerator, other industrial	1A1, 1A2	$deNO_x$ use in fossil fuel and MSW incineration plants	35.9±13.1	3.9±2.9	17.6±0.5	Ogawa et al. (2005a), Harris et al. (2015)
Transport	Agricultural and construction machinery, road traffic	1A3a, 1A3c, 1A3d, 1A3e, 1A3b	Fuel combustion in non-road transportation	28.6±9.9	-28.7±3.6	4.2±2.4	Toyoda et al., (2008)
			Fuel combustion for road transportation	40.3±3.7	-7.2±1.2	10.0±4.3	Toyoda et al., (2008)
Heating	Agricultural, commercial and private heating	1A4	Fuel combustion: other sectors (dominantly household heating)	37±10	5.5±6	3.5±4	Ogawa et al. (2005a), Ogawa et al. (2005b)
Refinery	Refineries	1B2a	Refineries	-	-	-	-
IndustryAndUse	Nitric acid production, use in households and hospitals	2 and 3	Nitric acid production (adipic acid, medical, and private (aerosol) use)	29.1±18.8	-8.3±10.6	3.3±5.5	Toyoda et al., (2008), Thiemens et al. (1991)
Manure	Manure management	4B	Manure management	23.9±3.8	-17.5±6.2	6.5±4.1	Maeda et al. (2010)
DirectAgri	Crop residues/soil organic matter, animal waste on pastures, synthetic fertilizer use, manure application	4C, 4D	Direct soil emissions	29.0±3.7	-17.8±5.7	7.2±3.8	Snider et al. (2015b), Wolf et al. (2015)
IndirectAgri	Leaching, other indirect emissions from agri. Soils	4D3	Direct soil emissions	29.0±3.7	-17.8±5.7	7.2±3.8	Snider et al. (2015b), Wolf et al. (2015)

WastBurning	Illegal waste burning	4F	Agricultural waste burning	25±3.0	-1.0±3.0	2.8±3.0	Ogawa et al. (2005b)
Waste	Industrial fermentation, wastewater treatment, sewage sludge burning	6	Waste (wastewater treatment)	31.5±14.1	-11.6±12.7	10.5±5.7	Snider et al. (2015b)
IndirectNat	Indirect emissions from (semi-)natural ecosystems	7B, and 7C	Indirect soil emissions	29.0±3.7	-17.8±5.7	7.2±3.8	Snider et al. (2015b), Wolf et al. (2015)

*Isotopic signatures for anthropogenic sources are obtained from the summary by Harris et al. (2017).

ᵠ These are the primary sources contributing to N_2O emissions in Switzerland

1036 **Table 2** Input variables for simple two-box model

Variable	Description	Value	Error distribution	References
m_{trop}	Air in the troposphere (mol)	1.5×10^{20}	Constant	Röckmann et al. (2003), Schilt et al. (2014)
m_{strat}	Air in the stratosphere (mol)	2.7×10^{19}	Constant	Röckmann et al. (2003), Schilt et al. (2014)
F_{ex}	Troposphere-stratosphere exchange rate (kg a^{-1})	$(5.37\pm1.26) \times 10^{17}$	Uniform	Röckmann et al. (2003), Schilt et al. (2014)
F_{ocean}	Oceanic N_2O flux (Tg a^{-1} N equivalents)	4±1	Gaussian	Schilt et al. (2014)
τ_{PI}	Preindustrial N_2O lifetime (year)	123±10	Gaussian	Prather et al. (2015)
τ_{PD}	Present day N_2O lifetime (year)	116±9	Gaussian	Prather et al. (2015)
c_{PI}	Mixing ratio in the preindustrial troposphere (nmol mol^{-1})	270±7.5	Uniform	Sowers et al. (2002), Röckmann et al. (2003)
$\delta^{15}N^{bulk}{}_{PI}$	Mean $\delta^{15}N^{bulk}$ of preindustrial tropospheric N_2O (‰)	8.9±2	Gaussian	Toyoda et al. (2013)
$\delta^{18}O_{PI}$	Mean $\delta^{18}O$ of preindustrial tropospheric N_2O (‰)	46.1±2	Gaussian	Toyoda et al. (2013)
$\delta^{15}N^{SP}{}_{PI}$	Mean $\delta^{15}N^{SP}$ of preindustrial tropospheric N_2O (‰)	19.05±2	Gaussian	Toyoda et al. (2013)
$\delta^{15}N_{ocean}$	Mean $\delta^{15}N^{bulk}$ for oceanic emissions (‰)	5.1±1.9	Uniform	Snider et al. (2015b)
$\delta^{18}O_{ocean}$	Mean $\delta^{18}O$ for oceanic emissions (‰)	44.8±3.6	Uniform	Snider et al. (2015b)
$\delta^{15}N^{SP}{}_{ocean}$	Mean $\delta^{15}N^{SP}$ for oceanic emissions (‰)	15.8±7.1	Uniform	Snider et al. (2015b)
$\delta^{15}N^{bulk}{}_{terr}$	Mean $\delta^{15}N^{bulk}$ for emissions from terrestrial soils (‰)	-16.7±11.2	Uniform	Snider et al. (2015b)
$\delta^{18}O_{terr}$	Mean $\delta^{18}O$ for emissions from terrestrial soils (‰)	30.1±9.6	Uniform	Snider et al. (2015b)
$\delta^{15}N^{SP}{}_{terr}$	Mean $\delta^{15}N^{SP}$ for emissions from terrestrial soils (‰)	10.1±11.2	Uniform	Snider et al. (2015b)

1037

Table 3 Trends of amospheric $\delta^{15}N^{bulk}$, $\delta^{15}N^{SP}$ and $\delta^{18}O$ at Jungfraujoch determined using discrete measurements between April 2014 and December 2018. The trends are determined for the whole dataset, the dataset filtered for free troposphere (removing data points with significant influence from plenary boundary layer) and the second-phase dataset with bi-weekly measurements (August 2016 to December 2018).

	$\delta^{15}N^{bulk}$ (‰ a^{-1})		$\delta^{15}N^{SP}$ (‰ a^{-1})		$\delta^{18}O$ (‰ a^{-1})	
	Raw	Deseasonalized	Raw	Deseasonalized	Raw	Deseasonalized
Whole dataset	-0.059±0.012*	-0.052±0.012*	0.069±0.029	0.065±0.027	0.020±0.011	0.019±0.011
Free troposphere	-0.060±0.014*	-0.054±0.013*	0.054±0.034	0.036±0.030	0.024±0.013	0.019±0.011
First phase (Apr. 2014-Feb. 2016)	-0.036±0.038	-0.041±0.035	0.449±0.100*	0.314±0.082*	0.238±0.029*	0.207±0.026*
Second phase (Aug. 2016-Dec. 2018)	-0.105±0.049	-0.130±0.045*	0.028±0.067	-0.007±0.066	-0.007±0.042	-0.001±0.040

* Indicate significance of linear regression.

Table 4 Results of the two-box model simulations and selected literature values for comparison.

	This study		RMSE[φ]	Sowers et al. (2002)[a]	Röckmann et al. (2003)[b]	Ishijima et al. (2007)[c]	Toyoda et al. (2013)[d]	Park et al. (2012)[e]	Prokopiou et al. (2017)[f]
Air sample age	NH[†]	NH(FT[η])		FA[†], IC[†]	FA	FA	NH	SH[†], FA	FA
	2014-2018	2014-2018		1785-1995	NA	1960-2001	1999-2010	1940-2005	1940-2008
α*	0.0154±0.004	0.0154±0.004	0.65 nmol mol^{-1}	0.0111 to 0.0128	NA	NA	NA	NA	NA
$F_{anth,2018}$ (Tg N a^{-1})	8.6±0.6	8.5±0.6	NA[†]	4.2 to 5.7	6.9	NA	5.5	6.6	5.4±1.7
$\delta^{15}N^{bulk}$-anth (‰)	-8.6±4	-8.5±4	0.23	-7 to -13	-11.4	-11.6	-9.84	-15.6±1.2	-18.2±2.6
$\delta^{18}O$-anth (‰)	34.8±3	34.3±3	0.22	17 to 26	31.7	NA	35.95	32.0±1.3	27.2±2.6
$\delta^{15}N^{SP}$-anth (‰)	10.7±4	10.7±4	0.50	NA	11.3	NA	8.52	13.1±9.4	18.0±8.6

[†] NH and SH: surface atmosphere from the Northern and Southern Hemisphere, respectively; FA: firn air; IC: ice core air; NA: not available.
[η] FT: Jungfraujoch dataset filtered for free troposphere (based on NO_y:CO).
* "Value" is the dimensionless constant α describing the exponential increase in the anthropogenic flux
[φ] RMSE refers to root mean square error. It is in nmol mol^{-1} for α, referring to the present day tropospheric mixing ratio for N_2O. For source isotopic values, RMSE is in the unit of ‰. Simulations with the whole dataset and the dataset filtered for free troposphere yielded the same RMSE.
[a] Estimates are for 1995.
[b] Estimates are for 1998; isotopic signatures of anthropogenic sources were calculated assuming modern tropospheric values to be the same as this study.
[c] Estimate is for 2000, for $\delta^{18}O$ calibration is not comparable.
[d] Estimates are for 2012 using the "Base" scenario.
[e] Estimates are for 2005.
[f] δ_{anth} values are averaged values for the period of 1940-2008.

Table 5 Isotopic signatures for the overall, anthropogenic and major N_2O sources contributing to N_2O variations at Jungfraujoch. Source signatures were estimated based on a "bottom-up" approach, with literature-derived isotopic signatures and fluxes for variable sources under the Swiss Meteotest emission inventory.

	Emission inventory (%)	$\delta^{15}N^{bulk}$ (‰)	$\delta^{15}N^{SP}$ (‰)	$\delta^{18}O$ (‰)	Reference
Overall source	100	-15.8 (6.2)	7.3 (3.9)	29.4 (5.5)	-
Anthropogenic source	89.4	-15.6 (6.3)	7.4 (4.0)	29.5 (5.7)	-
Agricultural emission	61.5	-17.8 (5.7)	7.2 (3.8)	29.0 (3.7)	Snider et al. (2015) Wolf et al. (2015)
Manure management	7.4	-17.5 (6.2)	6.5 (4.1)	23.9 (3.8)	Maeda et al. (2010)
Waste*	7.2	-11.5 (12.6)	10.4 (5.7)	31.3 (14.0)	Ogawa and Yoshida (2005) Snider et al. (2015)
Natural emission	10.9	-17.8 (5.7)	7.2 (3.8)	29.0 (3.7)	Snider et al. (2015) Wolf et al. (2015)

* "Waste" sources consist of both wastewater treatment and agricultural waste burning (biomass burning).

Figures

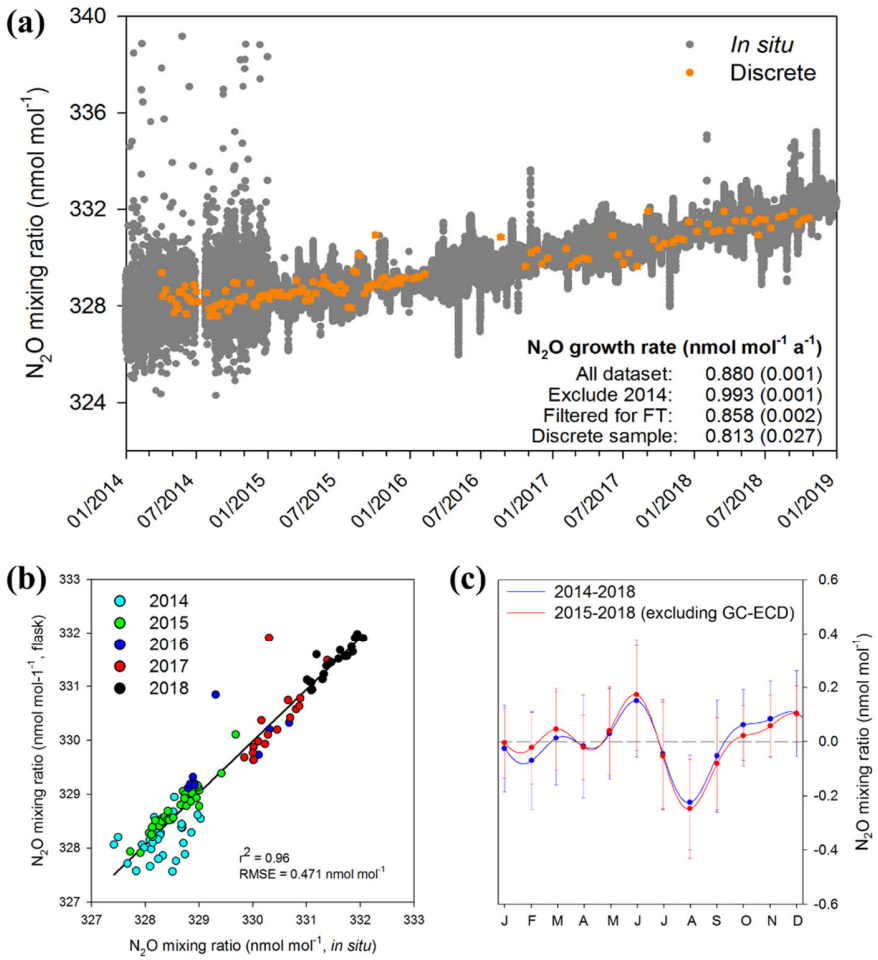

Figure 1a *In situ* (10-min averages) and discrete measurements of N_2O mixing ratios from April 2014 to December 2018 at Jungfraujoch. *In situ* N_2O mixing ratio measurements were performed with GC-ECD method between April and December 2014. After that, OA-ICOS became the major analytical method for *in situ* measurements. Discrete sample points are presented as averages with error bars (one standard deviation). Annual N_2O growth rates determined by linear regression are given in the figure (uncertainty shown as one standard deviation). A sampling gap exists for discrete samples between February and August 2016.

1b Comparison of in situ and discrete measurements of N_2O mixing ratios; in situ measurements were 10-minute values averaged over the exact period of discrete sampling time (~ 40 min); in situ measurements were performed with GC-ECD method in 2014, and this was replaced with OA-ICOS method from January 2015.

1c Seasonality of N_2O mixing ratios at Jungfraujoch derived from *in situ* measurements. Datasets with/without GC-ECD measurements are compared for seasonality evaluation. The NLS model simulation for time-series gives the detrended seasonality, with error bars indicating one standard deviation of monthly residuals.

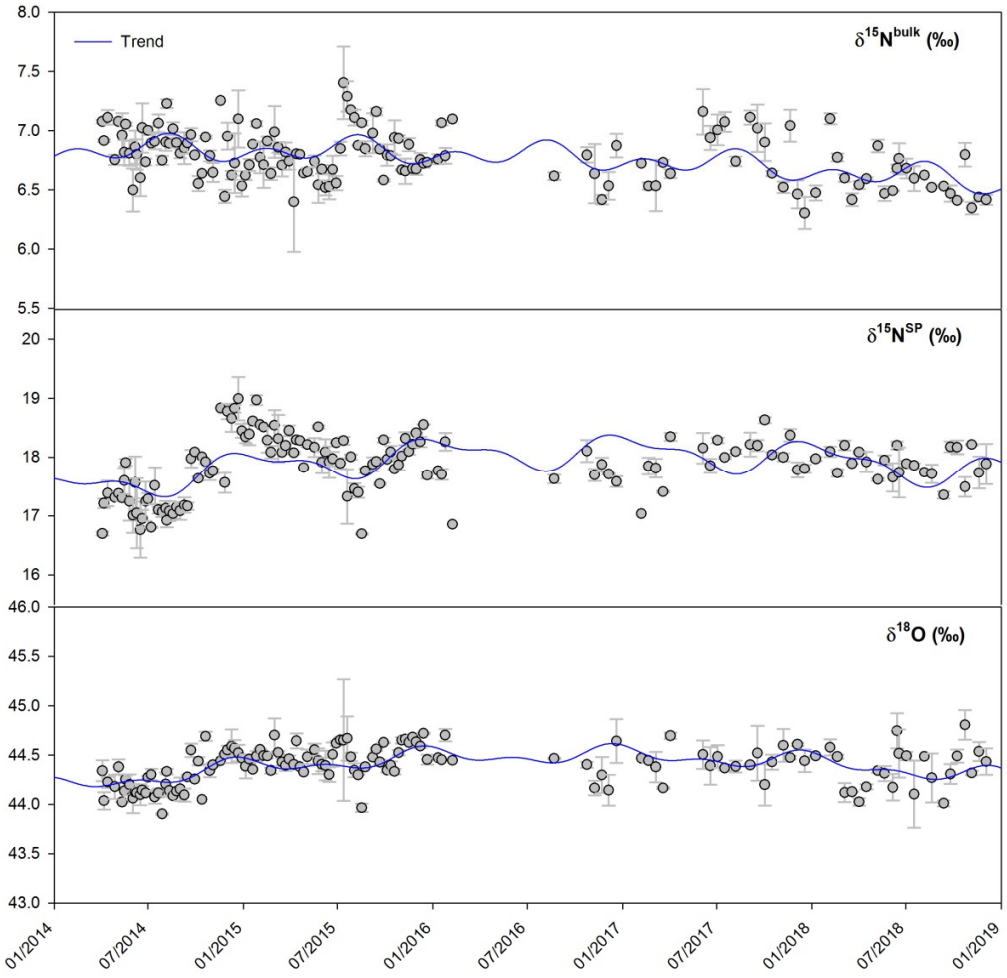

Figure 2 Time-series of isotopic composition of atmospheric N_2O observed at Jungfraujoch from April 2014 to December 2018. Error bars indicate one standard deviation of repeated measurements. Blue lines indicate the simulated trends by the NLS model.

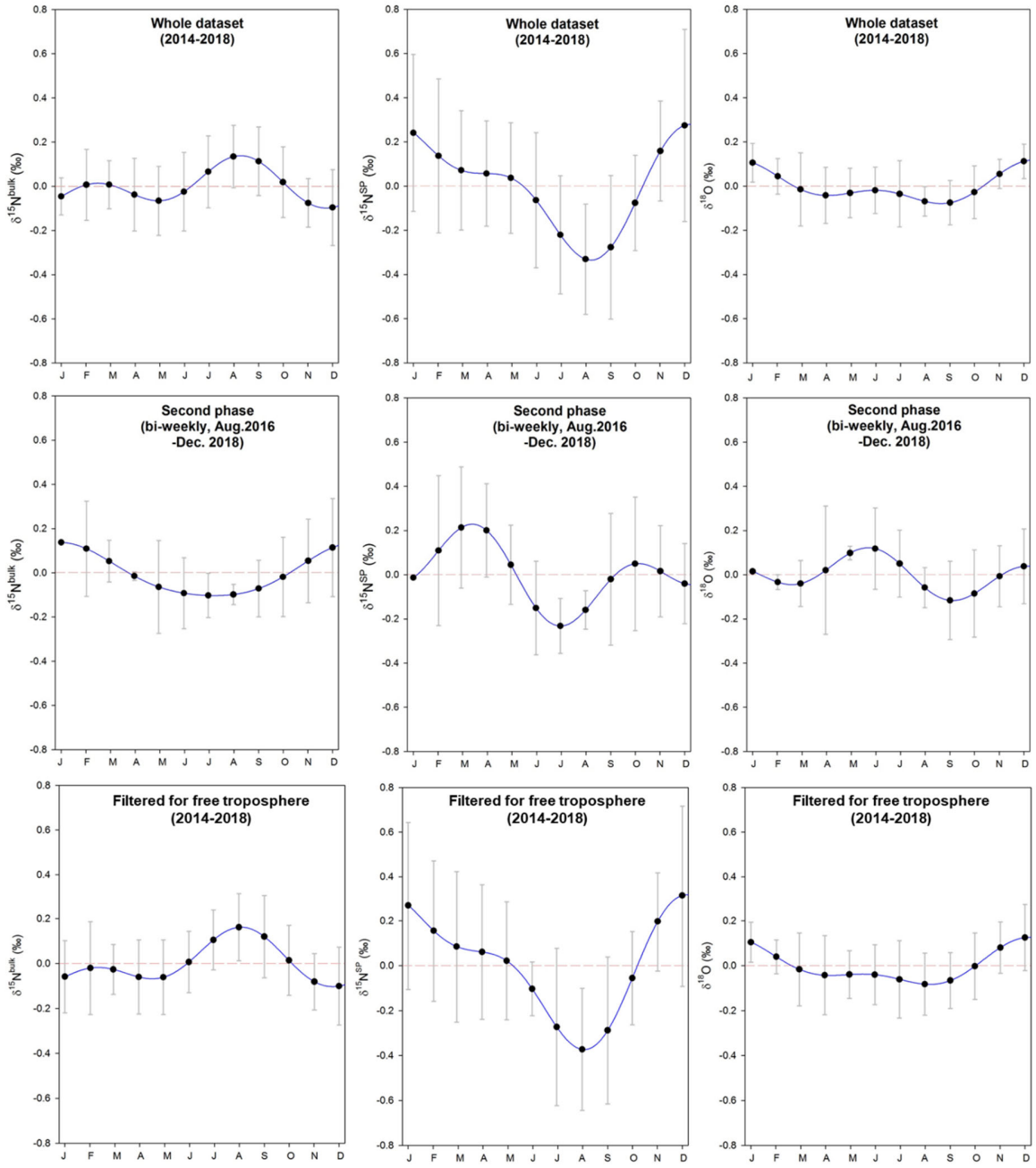

Figure 3 Seasonality of isotopic signatures of atmospheric N_2O observed at Jungfraujoch. Top panels: seasonality obtained using the whole dataset from April 2014 to December 2018; middle panels: seasonality obtained using bi-weekly data collected between August 2016 and December 2018; lower panels: seasonality obtained using dataset filtered for free troposphere from April 2014 to December 2018. Red dashed lines refer to zero variability. The NLS model simulation for time-series gives the detrended seasonality, with error bars indicating one standard deviation of monthly residuals.

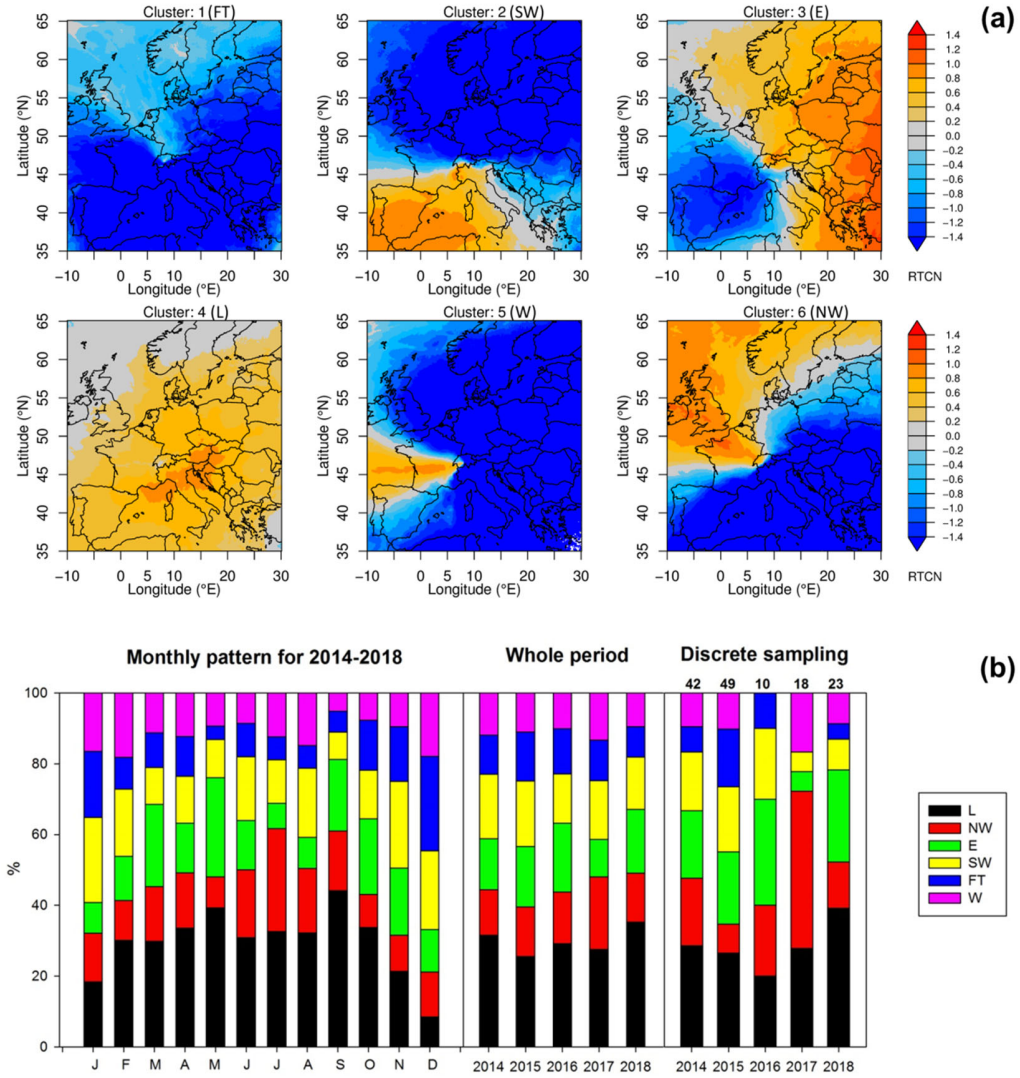

Figure 4a Clusters of air mass transport regimes for Jungfraujoch shown as normalized surface source sensitivities over our sampling period. Cluster abbreviations refer to Free Troposphere (FT), Southwest (SW), East (E), Local (L), West (W) and Northwest (NW). The normalization was done by calculating the difference between cluster average source sensitivity and whole period average source sensitivities, divided by the period average. Orange colors indicate the main source regimes in each cluster, whereas blue colors indicate little to no influence on Jungfraujoch observations. The free tropospheric cluster showed lower than average surface sensitivity everywhere.

4b Cluster frequency of air mass transport regimes (%) shown as a monthly pattern (left) and interannual patterns for the whole periods (middle) and for the periods of discrete sampling (right). Numbers above the right figure indicate the total number of discrete samples per year.

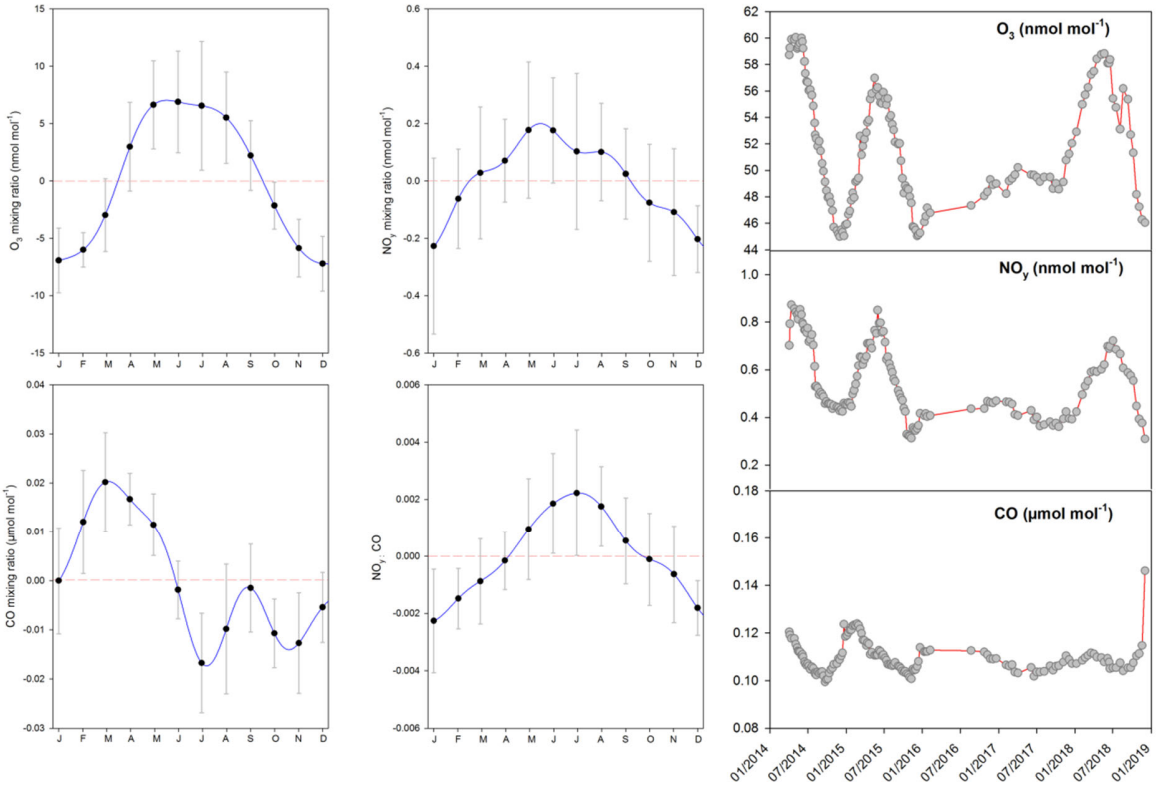

Figure 5 Left and middle: Seasonality of *in situ* measurements of O_3, NO_y and CO mixing ratios and NO_y/CO at Jungfraujoch; error bars represent the one standard deviation of monthly residuals from the NLS model simulation for time-series. 10-minute data were used for seasonality analysis.

Right: *In situ* measurements of O_3, NO_y and CO mixing ratios averaged over the exact period of discrete sampling (~40 min).

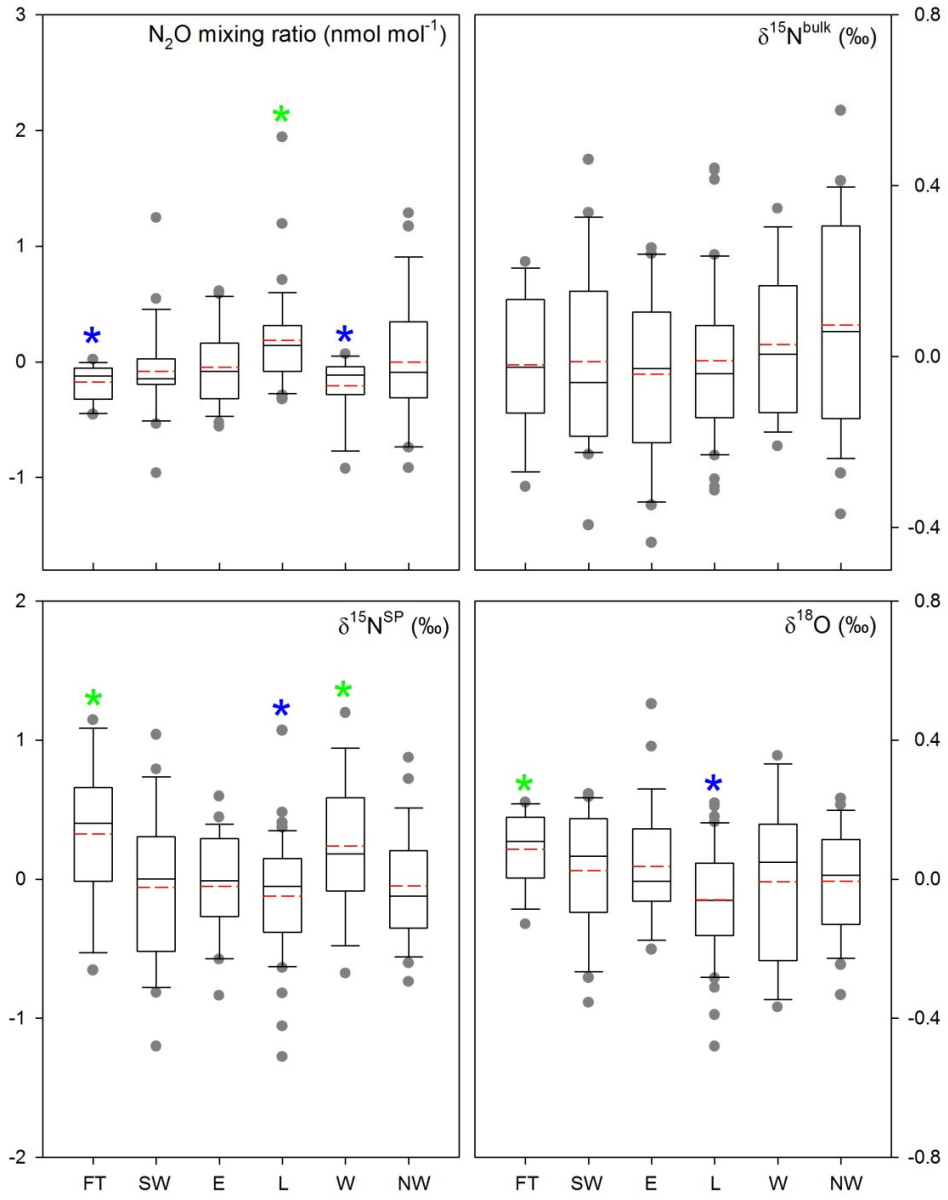

Figure 6 Comparison of N_2O mixing ratios and isotopic signatures (with linear trends removed) for the six air mass footprint clusters used in the present study. Green and blue stars indicate significantly larger and smaller values than the others, respectively; red dashed lines indicate mean levels; grey points indicate outliers.

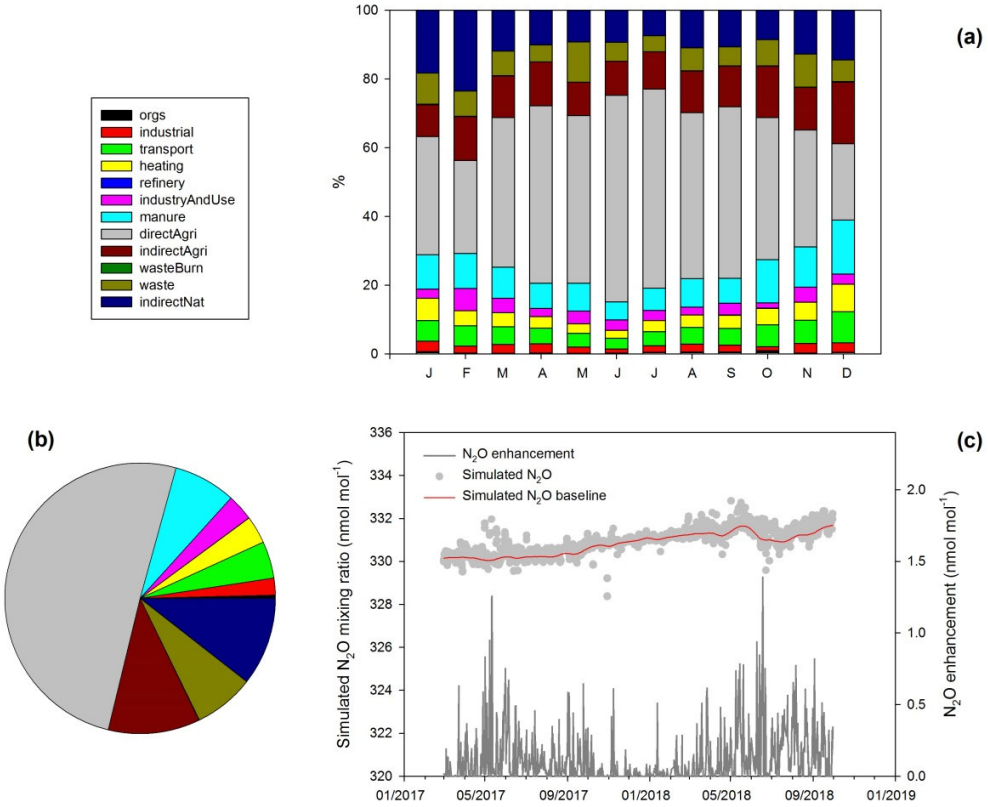

Figure 7a Mean monthly stacked-bar plots of source contributions (%) to atmospheric N_2O at Jungfraujoch derived from inversion modeling.

7b Overall contributions of N_2O sources responsible for emission to Jungfraujoch.

7c Simulated 3-hourly N_2O mixing ratios, N_2O mixing ratio baseline and N_2O enhancements in nmol mol^{-1}.

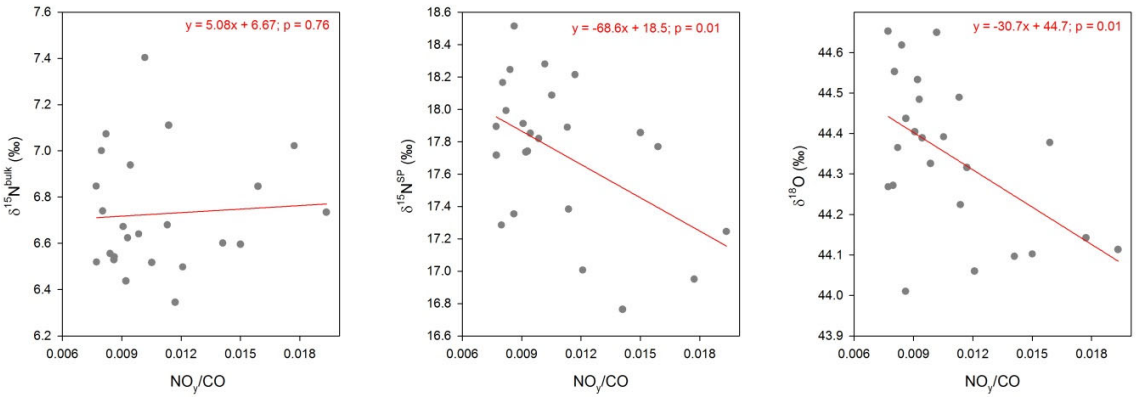

1125 **Figure 8** Relationship between the NO_y to CO ratios and isotopic signatures of N_2O; only data points with $NO_y/CO>0.007$ are presented here (which refers to scenarios with strong pollution from local air).

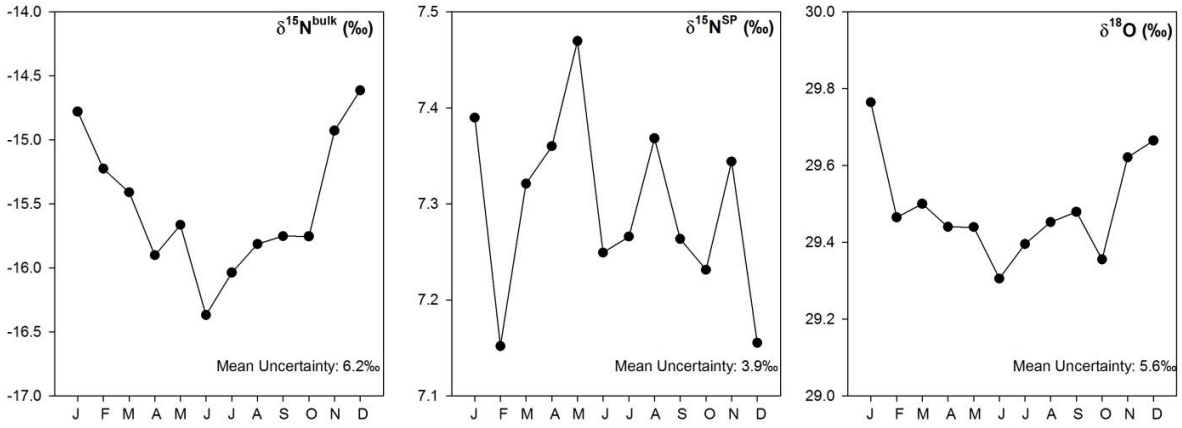

Figure 9 Simulated seasonal variations of isotopic signatures for overall N_2O sources based on the "bottom-up" approach; uncertainties shown in figures are comparable to the ranges of isotopic signatures for variable sources as found in literature.

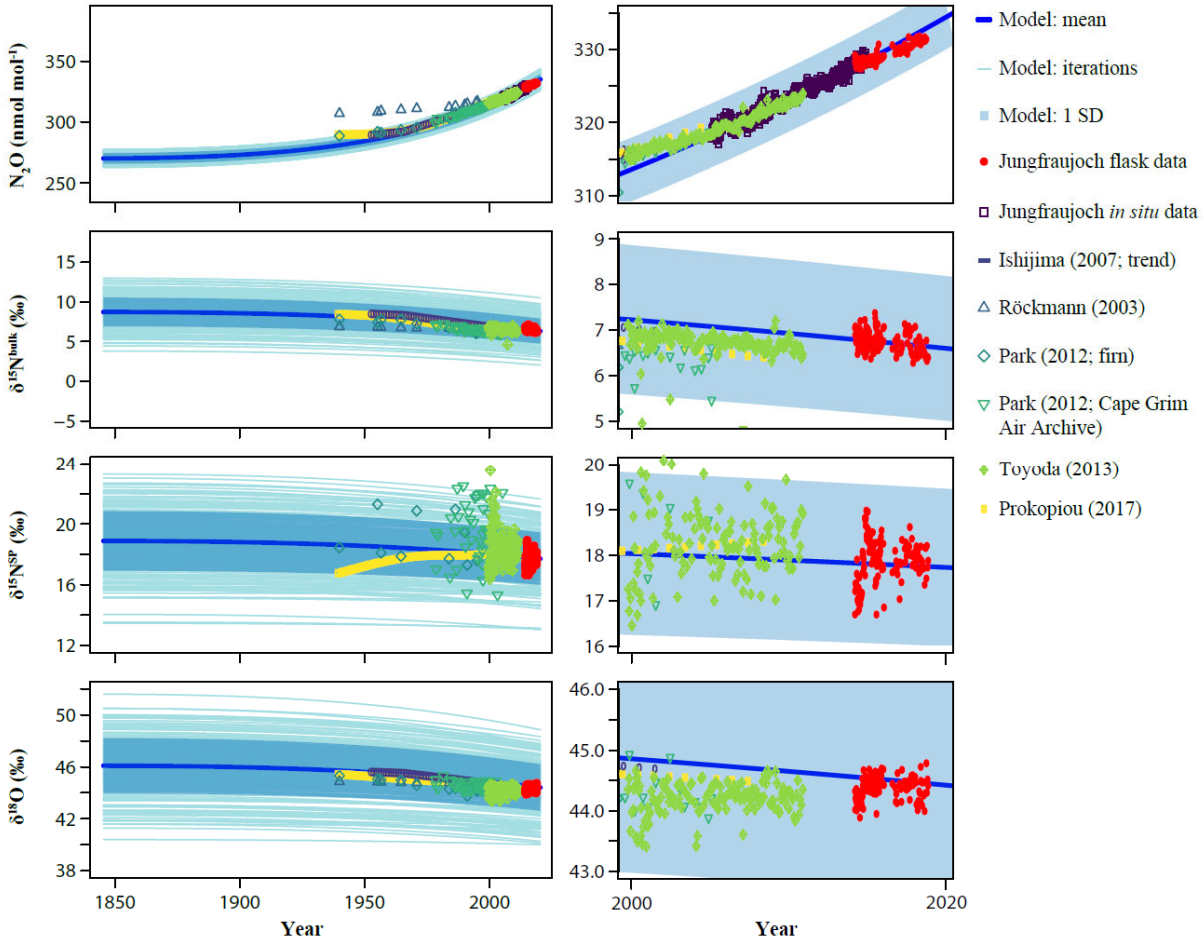

Figure 10 Two-box model results showing the influence of anthropogenic emissions on N_2O mixing ratio and isotopic composition in the troposphere. Left: full time range from the start of the anthropogenic period (1845) to present day; Right: zoom to the last two decades. Isotopic measurements at Jungfraujoch were used as the only constraint of current tropospheric N_2O isotopic composition for the model. See the materials and method as well as the SI for more details and other input parameters. Atmospheric as well as firn air measurements of $\delta^{15}N^{bulk}$, $\delta^{15}N^{SP}$ and $\delta^{18}O$ from the literature are presented for comparison. Blue shaded areas indicate one standard deviation of the model iterations.